

# Postseismic backslip as a response to a sequential elastic rebound of upper plate and slab in subduction zones

Ehsan Kosari<sup>1,1,1</sup>, Matthias Rosenau<sup>2,2,2</sup>, Thomas Ziegenhagen<sup>1,1,1</sup>, and Onno Oncken<sup>3,3,3</sup>

<sup>1</sup>Helmholtz Centre Potsdam, GFZ German Research Centre for Geosciences

<sup>2</sup>GFZ Potsdam

<sup>3</sup>GeoForschungsZentrum Potsdam

November 30, 2022

## Abstract

An earthquake-induced stress drop on a megathrust instigates different responses on the upper plate and slab. We mimic homogenous and heterogeneous megathrust interfaces at the laboratory scale to monitor the strain relaxation on two elastically bi-material plates by establishing analog velocity weakening and neutral materials. A sequential elastic rebound follows the coseismic shear-stress drop in our elastoplastic-frictional models: a fast rebound of the upper plate and the delayed and smaller rebound on the elastic belt (model slab). A combination of the rebound of the slab and the rapid relaxation (i.e., elastic restoration) of the upper plate after an elastic overshooting may accelerate the relocking of the megathrust. This acceleration triggers/antedates the failure of a nearby asperity and enhances the early slip reversal in the rupture area. Hence, the trench-normal landward displacement in the upper plate may reach a significant amount of the entire interseismic slip reversal and speeds up the stress build-up on the upper plate backthrust that emerges self-consistently at the downdip end of the seismogenic zones. Moreover, the backthrust switches its kinematic mode from a normal to reverse mechanism during the coseismic and postseismic stages, reflecting the sense of shear on the interface.

# Upper plate response to a sequential elastic rebound and slab acceleration during laboratory-scale subduction megathrust earthquakes

Ehsan Kosari<sup>1,2</sup>, Matthias Rosenau<sup>1</sup>, Thomas Ziegenhagen<sup>1</sup>, and Onno Oncken<sup>1,2</sup>

<sup>1</sup> Helmholtz Centre Potsdam, GFZ German Research Centre for Geosciences, Potsdam, Germany.

<sup>2</sup> Department of Earth Sciences, Freie Universität Berlin, Berlin, Germany.

Corresponding author: Ehsan Kosari ([ehsan.kosari@gfz-potsdam.de](mailto:ehsan.kosari@gfz-potsdam.de))

## Key Points:

- Seismotectonic scale models provide high-resolution observations to study the surface deformation signals from shallow megathrust earthquakes
- Surface displacement time-series suggest a sequential elastic rebound of the upper plate and slab during great subduction megathrust earthquakes
- Slip reversal may be caused by rapid restoration of the upper plate after overshooting and amplified upper plate motion

**Abstract**

An earthquake-induced stress drop on a megathrust instigates different responses on the upper plate and slab. We mimic homogenous and heterogeneous megathrust interfaces at the laboratory scale to monitor the strain relaxation on two elastically bi-material plates by establishing analog velocity weakening and neutral materials. A sequential elastic rebound follows the coseismic shear-stress drop in our elastoplastic-frictional models: a fast rebound of the upper plate and the delayed and smaller rebound on the elastic belt (model slab). A combination of the rebound of the slab and the rapid relaxation (i.e., elastic restoration) of the upper plate after an elastic overshooting may accelerate the relocking of the megathrust. This acceleration triggers/antedates the failure of a nearby asperity and enhances the early slip reversal in the rupture area. Hence, the trench-normal landward displacement in the upper plate may reach a significant amount of the entire interseismic slip reversal and speeds up the stress build-up on the upper plate backthrust that emerges self-consistently at the downdip end of the seismogenic zones. Moreover, the backthrust switches its kinematic mode from a normal to reverse mechanism during the coseismic and postseismic stages, reflecting the sense of shear on the interface.

**Plain Language Summary**

Subduction zones, where one tectonic plate slides underneath the other, host the largest earthquakes on earth. Two plates with different physical properties define the upper and lower plates in the subduction zones. A frictional interaction at the interface between these plates prevents them from sliding and builds up elastic strain energy until the stress exceeds their strength and releases accumulated energy as an earthquake. The source of the earthquake is located offshore; hence illuminating the plates' reactions to the earthquakes is not as straightforward as the earthquakes that occur inland. Here we mimic the subduction zone at the scale of an analog model in the laboratory to generate analog earthquakes and carefully monitor our simplified model by employing a high-resolution monitoring technique. We evaluate the models to examine the feedback relationship between upper and lower plates during and shortly after the earthquakes. We demonstrate that the plates respond differently and sequentially to the elastic strain release: a seaward-landward motion of the upper plate and an acceleration in the lower plate sliding

underneath the upper plate. Our results suggest that these responses may trigger another earthquake in the nearby region and speed up the stress build-up on other faults.

## 1 Introduction

Large megathrust earthquakes (i.e., slip) cause a shear stress drop on the subduction interface that drives the subduction system from a quasi-steady state interseismic loading stage (i.e., stick) to a temporarily non-stationary (i.e., transient) relaxation mode. Although the static coseismic and interseismic surface deformation of subduction megathrust has been analyzed in much detail (e.g., Chlieh *et al.*, 2008; Loveless & Meade, 2011; Moreno *et al.*, 2010; Schmalzle *et al.*, 2014; Simons *et al.*, 2011), the motion of the upper plate caused by the transition from coseismic to quasi-static interseismic deformation has received somewhat less attention (Bedford *et al.*, 2020). The spatial and temporal resolution of the near-source observations is the main challenge of dynamic instability analysis (Kosari *et al.*, 2020). The transition from coseismic phase to postseismic phase involves different mechanisms over the shallow (mainly offshore: up to 30 km) and deep (onshore: 30-90 km) parts of the subduction interface, which are rheologically dominated by elastoplastic (lithosphere) and viscoelastic (asthenosphere) behavior, respectively (e.g., Wang *et al.*, 2012; Weiss *et al.*, 2019). To date, several postseismic processes have been identified that can be seismic and aseismic, namely (1.) afterslip along the megathrust (e.g., Hsu *et al.*, 2006; Bedford *et al.*, 2013; Hoffmann *et al.*, 2018), (2.) viscoelastic relaxation of the lower crust and mantle of both slab and upper plate (e.g., Sun *et al.*, 2014; Li *et al.*, 2015) and (3.) crustal faulting in the upper plate (extensional), accretionary wedge (compressional), and shallow slab (extensional) (e.g., Kato *et al.*, 2011; Hicks and Rietbrock., 2015; Hoskins *et al.*, 2021). All these non-stationary mechanisms are triggered from coseismic stress changes (i.e., shear stress changes along the fault) on the interface; hence, the pattern of the stress changes and its magnitude and, on the other hand, the dynamics of the slip are the main controlling factors.

Only a handful of megathrust earthquakes are relatively densely monitored. In many of these cases, the early postseismic surface displacement above the ruptured asperity, which is remotely offshore, exhibits intriguing signals that are interpreted differently (e.g., Bedford *et al.*, 2016; Heki & Mitsui, 2013; Tomita *et al.*, 2017; Watanabe *et al.*, 2014). While the postseismic viscoelastic surface signal from the relaxing asthenosphere appears with a characteristic long-term pattern and large-scale

wavelength (far-field, hundreds of kilometers scale) (e.g., Luo & Wang, 2021; Sun & Wang, 2015; Wang et al., 2012), the postseismic elastic-frictional processes (i.e., relocking and afterslip) show relatively steep temporal gradients (i.e., fast changes) and short-wavelength (tens of kilometers scale) surface signals. The short-wavelength postseismic signals, typically manifested in sustained surface seaward motion, interfere in the near-field with the presumably steadier interseismic re-loading process that has a reverse kinematic sense (i.e., landward surface displacement in the upper plate). Such interference causes surface displacement above the ruptured patch and nearby regions to be characterized by short time and short distance changes in amplitude and direction, often causing local shear and vertical axis rotations in the surface displacement observations (e.g., Loveless, 2017; Melnick *et al.*, 2017; Yuzariyadi and Heki, 2021). . Moreover, it is not fully evident how the fast dynamic processes, i.e., changes in the rupture propagation direction, contributes to these surface displacement “enigmatic patterns” in the upper plate during the coseismic and early postseismic stages (Ide et al., 2011). Such patterns above the seismogenic portion of the interface in the upper plate are notoriously difficult to interpret mainly due to the limited observation resolutions (temporal and spatial), and discourse is rising about their relevance for seismic hazards. Unfolding the upper plate displacement over coseismic and early postseismic stages can straighten out the mainly frictional processes of the shallow (seismogenic portion) interface.

To study how the elastoplastic-frictional signals contribute to this intricate upper plate surface displacement, we here idealize a subduction megathrust system highlighting the potential variability of surface deformation signals over coseismic and early postseismic phases in subduction megathrusts. This study aims to address the sequential upper plate and slab elastoplastic-frictional response during the coseismic shear-stress drop and its early postseismic stage in a subduction megathrust system by employing a series of carefully monitored analog modeling experiments. Seismotectonic Scale Modeling can examine elastic and permanent deformation and investigate the interplay between short-term and long-term deformation signals in 3-D (Kosari et al., 2022a; Rosenau et al., 2009). To examine the short-term feedback relationship between the upper plate and the slab, we explore two generic seismotectonic models representing seismically homogeneous and heterogenous subduction megathrust systems and capture the

model's surface displacements by employing a high resolution and high speed “laboratory seismogeodetic” method.

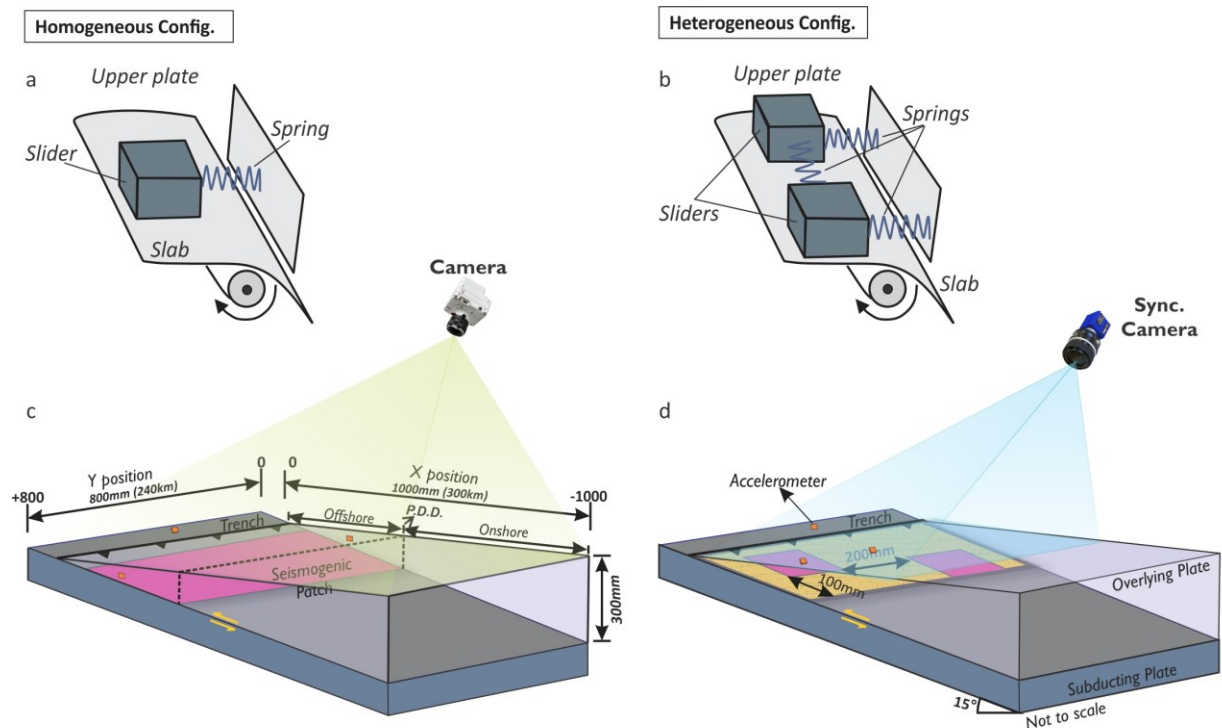


**Figure 1.** Scheme of the seismotectonic scale model's geometry and configuration: *a* and *b* demonstrate our conceptual systems of coupled spring sliders as depicted by Ruff and Tichelaar, (1996). *b* and *c* represent homogenous and heterogeneous configurations, respectively. The yellow (matrix) and magenta (main slip patch) rectangles demonstrate the seismogenic patches which generate repeating earthquake and megathrust events, respectively. P.D.D. represents the projection of the down-dip limit of the seismogenic patch on the model surface. The small orange rectangles show the different configurations of accelerometers. The frictional behavior of both velocity weakening materials used in the matrix and main slip patch is shown in Figure 2.

## 2 Methodology: Seismotectonic scale modeling

Seismotectonic scale models have been established to generate physically self-consistent analog megathrust earthquake ruptures and seismic cycles at the laboratory scale (Rosenau et al., 2009; 2017, and references therein). They have been used to study the interplay between short-term

elastic (seismic) and long-term permanent deformation (Rosenau & Oncken, 2009), slip variability (Rosenau et al., 2010), earthquake recurrence behavior and predictability (Corbi et al., 2020; 2019; 2017; Rosenau et al., 2019), the linkage between offshore geodetic coverage and coseismic slip model (Kosari et al., 2020) and to illuminate details of the seismic cycle (Caniven & Dominguez, 2021). Analog models are downscaled from nature for the dimensions of mass, length, and time to maintain geometric, kinematic, and dynamic similarity by applying a set of dimensionless numbers (King Hubbert, 1937; Rosenau et al., 2009; 2017). The models generate a sequence of tens to hundreds of analog megathrust earthquake cycles, allowing the analysis of the corresponding surface displacement from dynamic coseismic (e.g., Movi S2) to quasi-static interseismic in which inertial effects are negligible due to the slow deformation rates.

## 2.1 Experimental setup and material behavior

### 2.1.1 Model scaling and similarity

The small-scale laboratory models should share geometric, kinematic, and dynamic similarities with their prototype to be representative of a natural system as all lengths, time, and forces scale down from the prototype in a consistent way dictated by scaling laws (King Hubbert, 1937). According to Rosenau et al. (2009), we consider different timescales for coseismic and interseismic deformation phases. They introduced a “dyadic” timescale that recognizes two dynamically distinct regimes of the seismic cycle: the quasi-static interseismic regime, where inertial effects are negligible due to the slow deformation rates, and the dynamic coseismic regime, which is controlled by inertial effects. This allows us to slow down the earthquake rupture and speed up the loading phase, keeping dynamic similarity in both stages (Table S1).

In the quasi-static regime of the inter-seismic phase, scaling is identical to the typical scaling of long-term processes to the lab (Table S1). For long-term tectonic studies involving materials that deform brittle or viscous material, two dimensionless numbers, the Smoluchowski and Ramberg (Ramberg, 1967) numbers, are of interest according to the deformation regime. For a short-term time (i.e., coseismic and postseismic stages), Froude scaling is used to reach dynamic similarity (Rosenau et al., 2009). The model parameters without a dimension should be preserved, e.g., Poisson’s ratio  $\nu$ , the friction coefficient, and the friction rate and state parameters. An exception to this general scale in-dependence of dimensionless parameters is the moment magnitude  $M_w$ , which is related to the seismic moment (unit Nm) but is defined as being dimensionless. Here, we

scale up analog earthquake moment magnitude non-linearly by applying the scale factor of seismic moment (Rosenau et al., 2017). Typically, magnitudes of analog earthquakes are in the range of  $-6$  to  $-7$ , which correspond to earthquakes of  $M_w = 8-9$  in nature.

### 2.1.2 Model geometry and configuration of seismogenic zone

In the presented 3-D experimental setup modified from Rosenau *et al.* (2019) and introduced in Kosari *et al.* (2020, 2022a), an ocean-continent subduction forearc model is set up in a glass-sided box (1,000 mm across strike, 800 mm along strike, and maximal 300 mm deep) with a  $15^\circ$  dipping, elastic basal rubber conveyor belt hereafter “model slab”) driven at a constant rate by a DC motor via lateral rollers., normal to a rigid backwall. A flat-topped velocity neutral wedge made of an elastoplastic sand-rubber mixture (50 vol.% quartz sand G12: 50 vol.% EPDM-rubber) is sieved into the setup representing a 240 km long forearc segment from the trench to the volcanic arc (Figures 1).

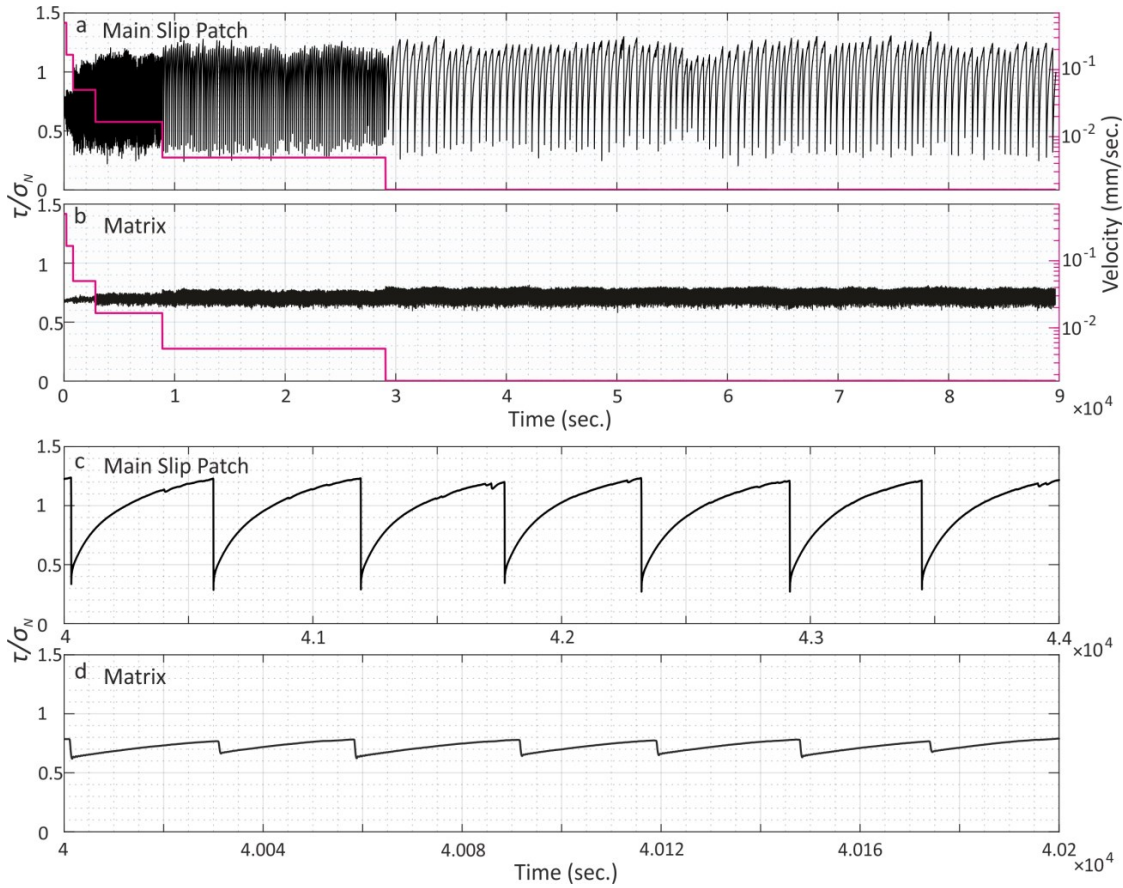
Before implementing the seismogenic zone in our seismotectonic model, we measure the rate-dependent material properties by the ring-shear tester RST-01.pc (Schulze, 1994). To estimate the friction rate parameter (a-b), the velocity stepping tests (VST; e.g., Pohlenz et al., 2020) in the RST carried out under constant normal load simulating coseismic and interseismic shear-stress drop and increases (Figure 2). At the base of the wedge, zones of velocity weakening controlled by granular stick-slip (“seismic” behavior) are realized by emplacing compartments of either sticky-rice (“main slip patches”) or fine-grained salt (“matrix”), which generate quasi-periodic large and small slip instabilities, respectively (Figures 1 and 2), mimicking megathrust earthquakes of different size and frequency. The VST demonstrates that large stick-slip instabilities in the main slip patch(es) (MSP) are almost complete (Figure 2c) and recur at low frequency (recurrence of the slip events:  $\sim 0.2$  Hz), while those in the matrix (Figure 2d) are partial ( $< 10\%$ ) and at high frequency ( $\sim 4$  Hz) at a prescribed constant normal load. This bimodal behavior is intended to mimic rare great ( $M8-9$ ) earthquakes versus small frequent repeating events (e.g., Uchida and Bürgmann, 2019; Chaves *et al.*, 2020) in a creeping environment akin to established concepts of the shallow subduction megathrust (e.g., Bilek and Lay, 2002). Note, however, that the quasi-



periodic recurrence of the small (scaling to M7-8) events might be an oversimplification, neglecting variability in this parameter in nature. In subduction megathrust, a rigid (oceanic) slab subducts beneath a wedge and forms a bi-material with a strong contrast megathrust interface. This contrasting results in different responses (e.g., strength drop) in the upper and lower plates coseismically (e.g., Ma & Beroza, 2008). In our model, the model elastic belt is stiffer than the wedge by a factor of 2-5. The wedge itself and the conveyor belt respond mainly elastically to these basal slip events, similar to crustal rebound during natural subduction megathrust earthquakes. Over the course of the experiment, the experiments evolve from an initially “aseismic stage” to a “seismic” steady-state (Kosari et al., 2022a; Rosenau et al., 2019). We select only the analog events from the seismically steady-state stage for our analysis. Upper plate faults (in our case, a single backthrust fault) gradually emerge self-consistently downdip and up-dip of the main slip patches and accommodate plastic upper plate shortening over seismic cycles, as documented in earlier studies (Kosari et al., 2020, 2022a; Rosenau et al., 2009, 2010, 2019; Rosenau & Oncken, 2009).

Two different seismic configurations of the shallow part of the wedge base (the megathrust) represent the depth extent of the seismogenic zone in nature. In the first configuration, hereafter named “homogeneous configuration”, a single large rectangular stick-slip patch (Width\*Length=200\*800 mm) is implemented as the main slip patch (MSP). This setup represents a system of a homogeneous seismogenic zone with temperature-controlled depth range and no variation along strike generating M9 type megathrust events such that the events rupture the stick-slip patch laterally uniformly. In the second case, hereafter named “heterogeneous configuration”, two square-shaped MSPs (200\*200mm) have been emplaced, acting as two medium-size seismogenic asperities (or discrete asperities (Herman & Govers, 2020)) generating M8-9 type events similar to, for example, the 2010 Maule (Chile) earthquake (Moreno et al., 2010). These two patches are at a center-to-center distance of 400mm and 100mm in trench-parallel and trench-normal directions, respectively, while surrounded by a salt matrix hosting frequent small events (Figures 1 and 2). To minimize the effect of boundary conditions, these MSPs are placed at a

reasonable distance (100mm), which is established experimentally (i.e., pilot experiments), from the sidewalls.



209

**Figure 2.** Shear stress time-series measured in a ring-shear tester during velocity stepping tests under constant normal load (2000 Pa). Stick-slip behavior simulates “seismic cycles” with coseismic and interseismic stress drop (analog earthquakes) and increase. a and b (main slip patch in Figure 1) and magenta (matrix in Figure 1) demonstrate the seismogenic (i.e., stick-slip) patches which generate megathrust events and repeating earthquakes, respectively. c and d show seven seismic cycles from both materials. Note that the recurrence of the repeating earthquake is approximately 20 times shorter than the megathrust event. If scaling is applied to these test data, one second corresponds to 250 years, stress drops would be 10-100 MPa, and friction coefficients consistent with Byerlee friction for the interseismic (~0.6-

0.7) and  $\sim 0.2$  after relocking. Note that we cannot measure friction during catastrophic failure properly in this kind of test.

## 2.2 Experimental monitoring: Laboratory seismogeodesy

A combination of seismological and geodetic methods applied to laboratory-scale models allows us to monitor the model's deformation at high spatial and temporal resolution and derive observational data equivalent to natural observations.

### 2.2.1 Laboratory geodesy

To capture horizontal micrometer-scale surface displacements associated with analog earthquakes at microsecond scale periods, we monitor the model surface with a highspeed CMOS (Complementary Metal Oxide Semiconductor) camera (Phantom VEO 640L camera, 12 bit, 4 MPx) intermittently at 250 Hz (Figure 1). A complimentary high-speed camera (200 Hz) is added to the monitoring system for synchronizing with the accelerometer. This synchronization allows differentiating the potential quasi-harmonic oscillations caused by dynamic frictional instability (i.e., coseismic) from event signals. Digital image correlation (e.g., Adam et al., 2005) has been applied at high spatial resolution ( $\sim 0.02$  mm) via the DAVIS 10 software (LaVision GmbH, Göttingen/DE). Data are processed to yield observational data similar to those from an ideal dense and full coverage (on- and offshore) geodetic network, that is, velocities (or incremental displacements) at locations on the model surface. We use an analog geodetic slip inversion technique (AGSIT; Introduced in Kosari et al., 2020) to invert surface displacements for model megathrust slip and backslip distribution over earthquake cycles. To tie slip/backslip in discretized fault patches to the observed surface displacement vectors (derived from DIC) at individual surface points, Green's functions for rectangular dislocations in an elastic half-space are computed and applied, and the dip-slip vector is solved for each patch (number of observations > number of fault patches). This provides an estimated slip of the shear plane formed in the velocity-weakening material. Although we do not consider the slip on the boundaries in our interpretations, we make the fault model larger than the model slab to avoid unreasonable estimated slip. Note that although

all observations can be upscaled to nature using scaling laws (King Hubbert, 1937; Rosenau et al., 2009, 2017), we here report all values at the laboratory scale.

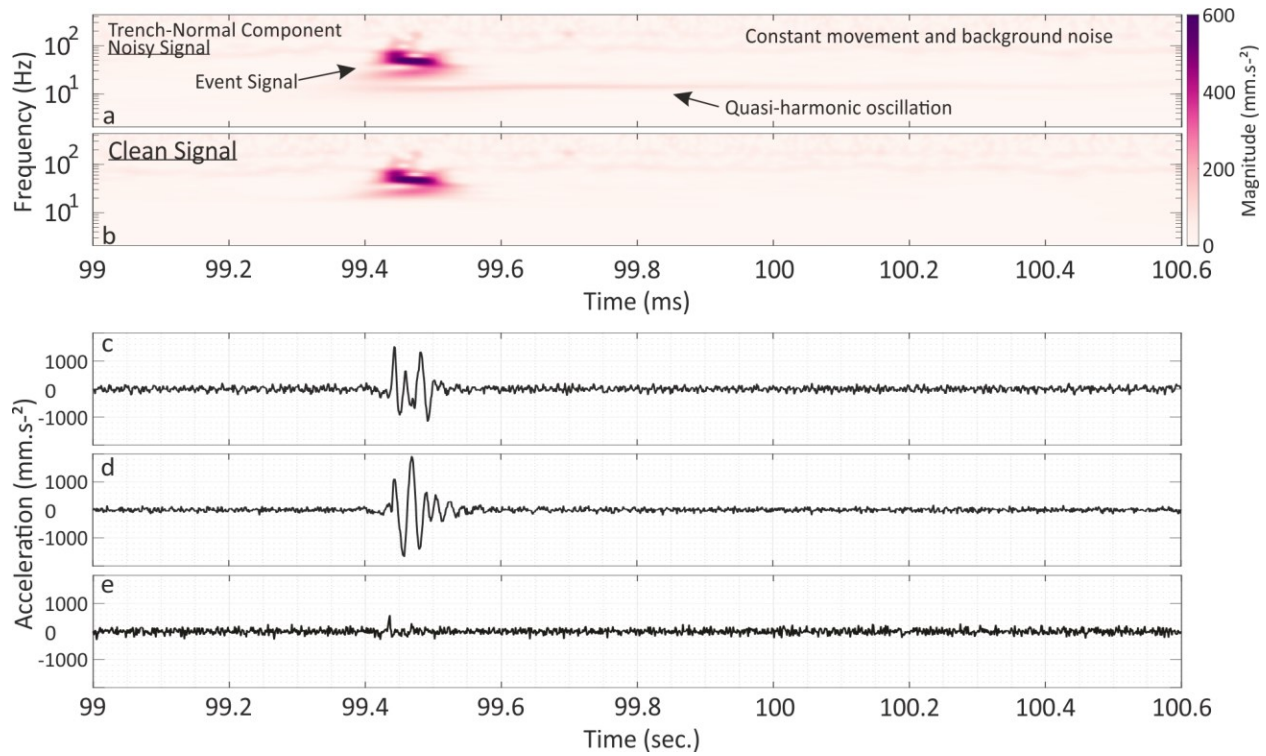


**Figure 3.** Differentiating Quasi-harmonic oscillation and event-related signals. *a* and *b* represent the scalogram of the signal before and after filtering the quasi-harmonic oscillations out. *c* and *d* are the normal-trench acceleration derived from three sensors located on the wedge (*c* and *d*) and the basal rubber conveyor belt (*e*).

### 2.2.2 Laboratory seismology

The experiments are additionally monitored using triaxial capacitive accelerometers (MEMS: microelectromechanical systems). The sensors (disynet DA3102) can measure with a sampling frequency of 10 kHz and a measuring range from 0 to  $\pm 2$  g. The bandwidth of the sensors depends on the sensor type and axis, ranging from 500 Hz to 1500 Hz. We positioned three sensors in different configurations to cover any possible motion in the setup (Figure 1), from the coseismic surface motions to the harmonic oscillations. The sensors run at 1 kHz to avoid the aliasing effect,

and a highpass filter has been applied to remove the quasi-harmonic oscillations from the waveform (Figure 3).

### 3 Results: Observations and interpretations

In the following, we analyze the high-resolution time-series of the surface and the model slab displacements and slip along the megathrust and an emergent upper plate fault over several seismic cycles. We analyze the heterogeneous model in-depth (compared to the homogeneous configuration) to capture the details of the upper plate and elastic belt responses in the coseismic and early-postseismic stages (Figures 4 & 7). We consider the Coulomb Failure Stress Change ( $\Delta\text{CFS}$ ) over coseismic and early-postseismic stages and its impact on model slab velocity changes (Figures 5). We calculate  $\Delta\text{CFS}$  to evaluate how the coseismic stress changes may trigger the slip reversal (backslip or normal faulting?) as well as how slip and backslip on the MSPs may transfer stress on the upper plate fault. Subsequently, we evaluate the elastic rebound of the model slab and the upper plate in response to the mainshock-induced stress changes. Finally, we explore the combined effect of the stress changes and elastic rebounds on the accumulation of the horizontal displacement in the upper plate and earthquake triggering (Figure 10).

#### 3.1 Kinematic observations and interpretations

##### 3.1.1 Time-variable surface displacements and slip over an analog earthquake and the early postseismic

As the recorded signals may occur at different scales, the scalogram of the synchronized accelerometer has been used to differentiate coseismic surface displacement versus machine-related oscillation and quasi-harmonic oscillations caused by dynamic frictional instability (Figure 3). The scalogram shows the absolute value of the waveforms, plotted as a function of time and frequency. The high-frequency signals ( $>60$  Hz) include the constant vibration of the machine and background noise. The slip event's elastic wave frequency ranges from 20 to 60 Hz, and the lower values ( $<20$  Hz) represent the event-triggered quasi-harmonic oscillations. The oscillation is removed from the signals using a highpass filter. The timing of each snapshot from the

synchronized camera is marked on the cleaned waveform to disregard the oscillation, and accordingly, 20 snapshots are selected to cover the coseismic and early-postseismic stages.

Figures 4c and d visualize the swath profiles of the cumulative surface displacements over the area above the seismogenic zone along the strike of the megathrust for both configurations (see Figures S1 & S2 for 2D surface displacement map). Figure 5a-b shows corresponding snapshots of the inverted slip along the megathrust and upper plate fault (antithetic to the megathrust) inverted from surface

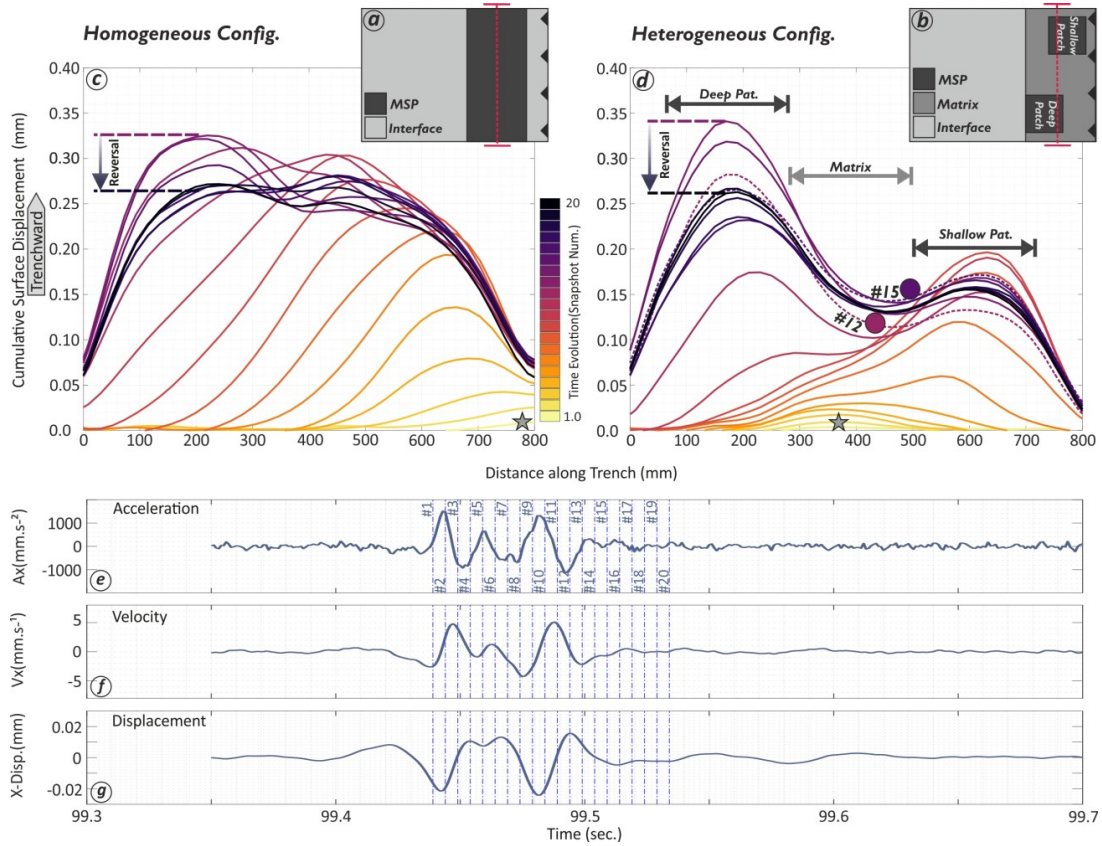


**Figure 4.** Model setup and exemplary evolution of coseismic and early-postseismic surface deformation in two scenarios. *a* and *b*: Plan view of the seismotectonic scale models' configurations; Light, medium, and dark gray colors represent the “aseismically” creeping interface, a velocity weakening matrix characterized by microslips (“microseismicity”), and the main slip patch(es) (MSP) where large analog megathrust earthquake slip occurs (“seismogenic zone” or “asperity”), respectively. The red dashed lines (marked by circles) show the profiles along which the cumulative surface displacement is shown in *c* and *d*. The gray star represents the location of the initiation of the rupture. The downward vectors indicate the

299 *reduction of the cumulative trenchward surface displacement representing surface displacement reversal*  
300 *during the early-postseismic stage interpreted as backslip. The corresponding surface deformation maps*  
301 *derived from the synchronized camera are visualized in figures S1 and S2. The stars on the dashed lines*  
302 *show the selected surface displacement snapshots for slip modeling in Figure 5. e-g show an exemplary*  
303 *acceleration, velocity, and displacement of the one sensor located on the wedge (Figure 2c). The timing of*  
304 *each snapshot has been marked on the waveforms.*

305 displacements. In the homogeneous system, the rupture initiates at the along-strike periphery of  
306 the stick-slip zone, grows radially in a crack-like fashion, and then laterally propagates as a pulse  
307 across the stick-slip zone (Figures 4c and S1). While the rupture arrests on the opposite side, the  
308 early rupture area seems to have relocked and apparently accumulates backslip at an even higher  
309 rate than the plate convergence rate. We term this kinematic observation “postseismic slip  
310 reversal” as it appears as a normal faulting mechanism (blue color in Figure 5b) in its formal  
311 inversion. Alternatively, the observation could also be explained by locking of the interface (no  
312 slip) combined with transient model slab acceleration (i.e., slab elastic rebound) triggered  
313 coseismically (see sections 4.2 and 4.3 for discussion). Whatever the source, the slip reversal is  
314 short-lived and propagates along the interface as the pulse behind the rupture. At the surface, this  
315 early instantaneous backslip (slip reversal) on the megathrust reduces the cumulative trenchward  
316 surface displacement (Figure 4c). The lack of significant afterslip in the MSPs and the matrix  
317 immediately after the coseismic stage and the landward surface displacement of the upper plate  
318 suggests a nearly complete stress-drop allowing the MSP and matrix to enter the relocking phase.

319 In the heterogeneous system, the rupture nucleates in the matrix, where a small foreshock event  
320 first triggers the failure of the shallow patch, followed by the failure of the deeper patch (Figures  
321 4d and S2). Because of the limited along-strike dimension of the MSP, megathrust failure occurs  
322 as a sequence of two discontinuous crack-like failures in contrast to the more continuous pulse-  
323 like failure in the uniform model. Again, a postseismic slip reversal occurs in the shallow MSP  
324 while the deep MSP is still in the process of failing (Figure 5a) and where slip reversal occurs  
325 slightly later. The landward displacement of the upper plate predominantly occurs above the site



of the two moderate-size MSPs. In other words, the MSPs, which host large slips, undergo larger postseismic slip reversal than the matrix.

### 3.1.2 Upper plate displacement accumulation

In both configurations, the postseismic backslip initiates immediately following the main event on the patches. The maximum amount of the backslip-caused surface displacement could reach 30% of the maximum coseismic surface displacement. The trench-normal surface displacements of the

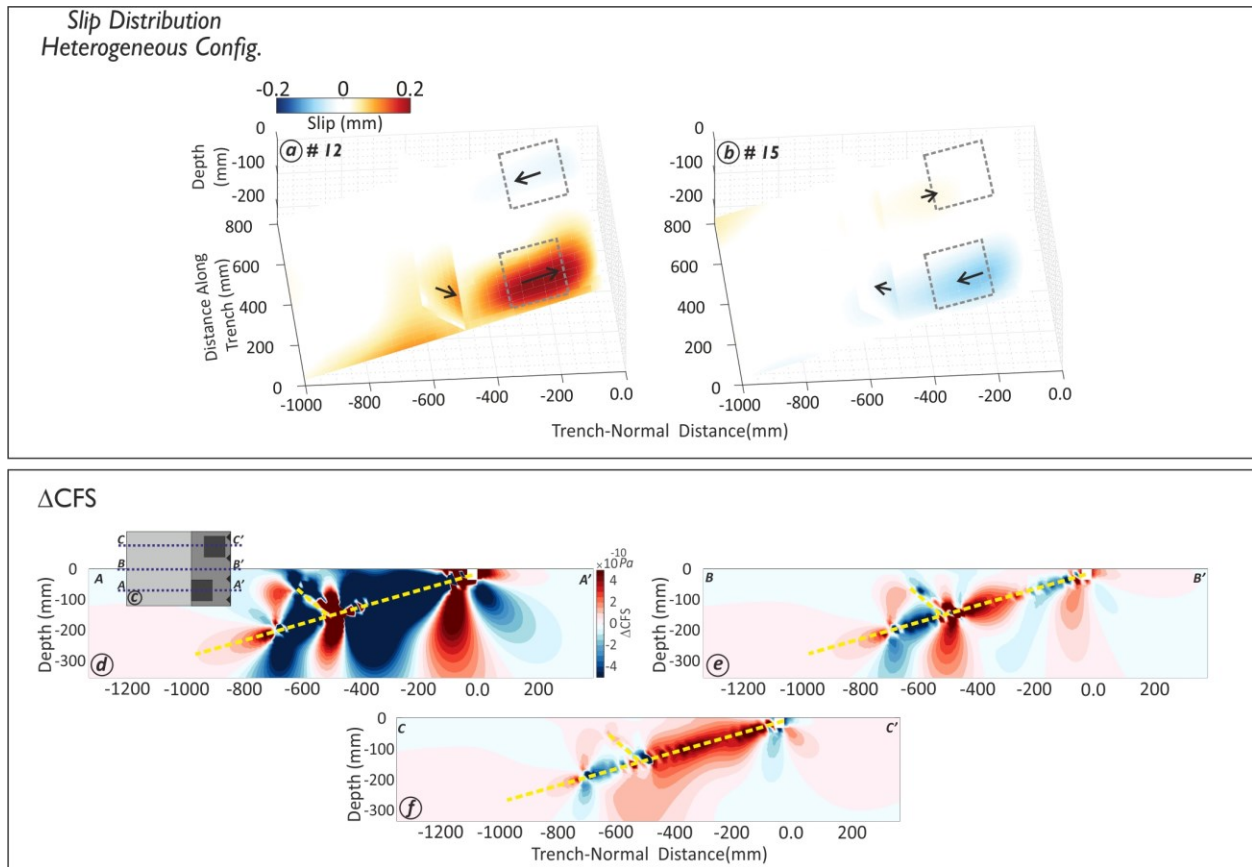


**Figure 5.** Upper panel: Slip models of the selected increments (marked in Figure 1d) in the heterogeneous system for demonstrating slip/backslip distribution in the MSPs and the antithetic upper plate fault. The vectors indicate the relative sense of slip but are not to scale. The dashed rectangles indicate the approximate location of the MSPs before shearing into trapezoids. The lower panel represents three trench-normal profiles of Coulomb failure stress changes ( $\Delta\text{CFS}$ ) from the slip model snapshot #12 in the heterogeneous configuration. Inset shows the location of profiles on the model surface.



coseismic, postseismic, and interseismic stages of an earthquake cycle have been visualized in Figure S5. Comparing the magnitude of the cumulative surface velocities reveals that the horizontal surface displacement (mostly seafloor in nature) during the early parts of the postseismic stage could reach up to 20-30% of the entire interseismic backslip.

Backthrusts accommodating long-term permanent wedge shortening and uplift emerge in the upper plate in both configurations during the model evolution. They are rooted in the down-dip limit of the stick-slip patch(es), where compressive stresses peak along the plate interface during the interseismic period.

We observe a kinematically consistent reactivation of the backthrust, i.e. as a normal fault during the coseismic megathrust slip phase and as a thrust in response to backslip on the megathrust. A slip ('trenchward') or backslip rearward ('landward') on the interface may re-activate the antithetic fault in the upper plate with a normal (e.g., #12 in Figure 5a) and/or a reverse sense of movement (e.g., #15 in Figure 5b), respectively. Following the slip distribution model (Figure 5a & b), two segments of the upper plate fault may move in opposite directions. This behavior likely reflects the shear sense on the MSPs. Particularly, in the upper plate fault, which in our experiments is rooted in the plate interface at the down-dip end of the seismogenic zone, the sense of slip (slip/backslip) on the seismogenic zone directly controls the slip mechanism of the antithetic fault. Based on the antisymmetric part of the two-dimensional velocity gradient tensor, we calculate the vertical axis rotation of the upper plate (Figure 6, the methodology can be found in Allmendinger et al., 2007). The uniform and dense distribution of the observation points at the model surface allows us to use the nearest neighbor points to calculate each point's rotation around a vertical axis. In the case of coseismic trenchward displacement of the upper plate, a divergent motion in the surface velocities above the rupture zone leads to a (sub-) symmetric vertical rotation while it may also rotate the adjacent areas. However, there is no significant rotation above the nearby (deeper) asperity. On the other hand, in the stage that the MSPs are on opposite modes (loading vs. unloading), the surface velocities above the loading MSP show a convergence mode as it may enhance the shortening rate in the early postseismic stage.

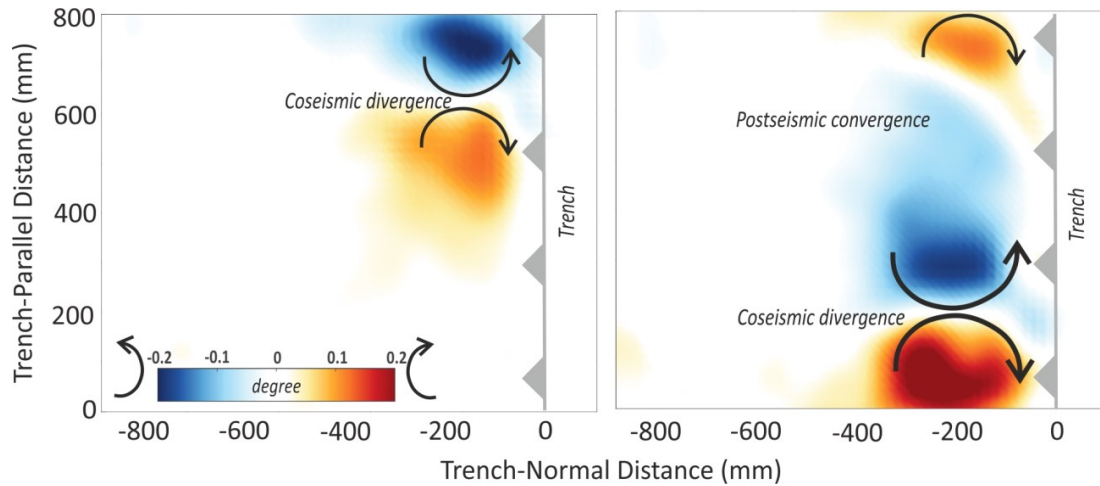


**Figure 6:** Exemplary clockwise and anticlockwise upper plate rotation during coseismic and early postseismic stages derived from selected surface displacements increments. Their associated surface displacements (E07 and E11) are visualized in Figure S2. Note that the sense of rotation during coseismic and postseismic stages causes divergence and convergence motion above the MSPs in the upper plate.

### 3.2 Interpretation of the dynamics: Coulomb failure stress changes

To constrain the triggering dynamics, we consider static stress changes in our models. Based on the slip and backslip pattern documented above, we derive Coulomb failure stress changes ( $\Delta\text{CFS}$ ) (e.g., Lin and Stein, 2004) induced by the mainshock on the megathrust and the antithetic fault to get insight into zones of enhanced/decreased CFS (lower panel in Figure 5 and S3). We calculate the  $\Delta\text{CFS}$  for the coseismic and postseismic stages of an event for the heterogeneous system on the receiver faults with the same sense and orientation as slip (thrust receiver faults in Figure 5) and backslip (normal receiver faults Figure S4) on the interface. In the shallow part of the plate interface (profile c-c'), a negative  $\Delta\text{CFS}$  lobe is bounded by two positive  $\Delta\text{CFS}$  lobes. The  $\Delta\text{CFS}$  is highly enhanced at the upper limit of the rupture, where the shallow part of the interface ruptures and is adjacent to the main slip zone on the slab. The  $\Delta\text{CFS}$  on the normal receiver fault (Figure S3) shows a decrease and an increase at the up-dip limit of the deep (in slip phase) and shallow (in backslip phase) MSPs on the slab, receptively.

Another lobe of positive  $\Delta\text{CFS}$  is extended to the down-dip limit of the main rupture area, where the antithetic fault in the upper plate appears during the model evolution (Figure 5). The deep-rooted antithetic fault, which imposes a significant discontinuity in the upper plate, perturbs the

inner-wedge stress state and highly increases the CFS at the conjunction of the interface and the antithetic fault. Hence, it builds up stress and enhances the  $\Delta\text{CFS}$  in the upper plate. However, the uncertainties in the slip distribution models at the conjugation zone may affect the  $\Delta\text{CFS}$ 's uncertainty. A relatively strong increase in CFS is predicted for the deeper MSP. Likely, it results from a combination of backslip on the deeper MSP and the mainshock-induced stress transfer.

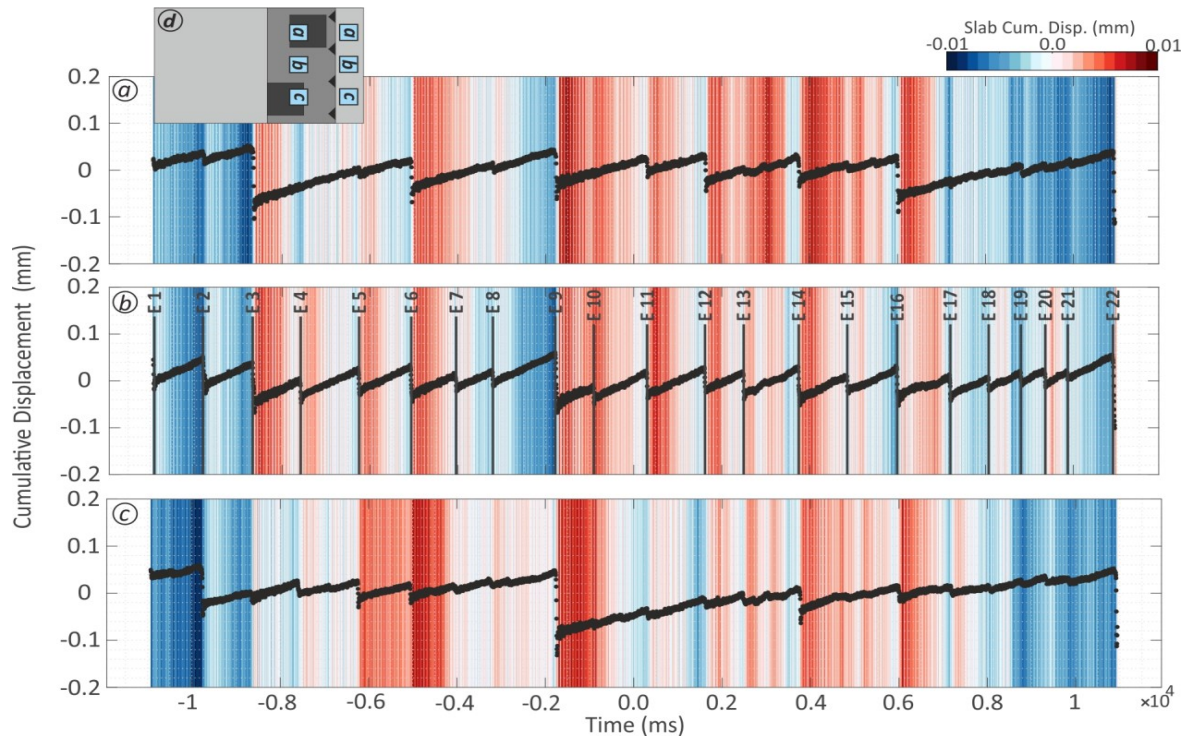


**Figure 7.** Upper plate time-series overlaid on the model slab time-series (background colormap) from the heterogeneous configuration (see Figure S4 for the homogenous configuration). Note the location of the profiles relative to the upper plate and slab. The vertical lines (E1-E22) indicate abrupt surface displacement changes above the matrix. The warm color shows the landward displacement of the slab. Larger events instigate greater model slab responses (Figure 8).

## 4 Discussion

### 4.1 Sequential elastic rebound of upper plate and slab?

We combine kinematic and dynamic results to shed light on the mechanism active during an analog earthquake. We analyze and interpret the cumulative displacement fields of a few earthquake cycles for both configurations to reach an accurate view of the elastic responses from the model slab and upper plate to the stress drop on the interface (Figure 7 & S4). Starting simple and in line

with the *elastic rebound theory* (Reid, 1910), the coseismic strain energy release (i.e., shear-stress drop) leads to the rebound of the interseismically strained upper plate and slab and transfers stress to the adjacent and nearby regions. The elastic response manifests itself in the strain energy converted to kinetic energy and consumed to accelerate the upper plate and (subordinately) the slab. The rebounds on the upper plate and slab (i.e., opposite sides of the megathrust interface) are in opposite directions (Savage, 1983). When we examine the velocity changes of the plates, we find that the model slab accelerates landward (Figures 7 & S4). The slab velocity increases by 50%-300% of the long-term velocity co- and early postseismically, depending on the event's magnitude. The magnitude of the events and model slab accelerations indicate a positive correlation: the larger the earthquake, the stronger is the response generated (Figures 7 & 8). While we cannot measure the elastic rebound of the slab in the asperity area on the interface directly, these values should be considered minimum values of local slab acceleration.

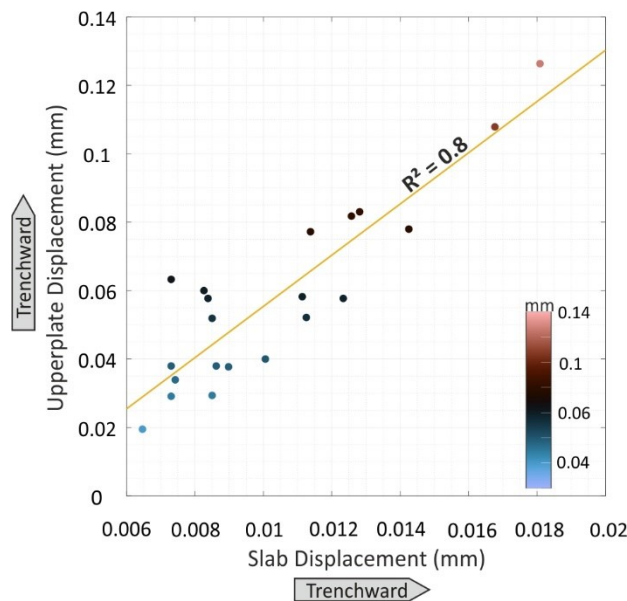


**Figure 8.** Correlation between the upper plate and model slab trenchward (landward) displacements during coseismic and early-postseismic stages.

Im et al. (2019) and Im & Avouac, (2021) show that the transition from a quasi-static stick-slip to a harmonic oscillation can be described by the emergence of dynamic instability. In a single-degree-of-freedom spring-slider system, the latter tends to become unstable for a larger mass or velocity and is sensitive to the loading velocity representing the contribution of inertia to frictional

instability. In the cases that the inertial instability is high or normal stress is low, friction-induced vibration (harmonic oscillation) may appear in any system exhibiting velocity weakening friction. Comparable with nature, the normal load in the shallow part of the subduction megathrust (i.e., the offshore portion in nature) is sufficiently low (Gao & Wang, 2017) and does not undergo relevant change during the coseismic period. However, the velocity increases significantly due to coseismic slip on the interface. These normal stress and velocity conditions prompt the system, which is already in unstable mode (i.e., slip), to the domain (Figure 1 in Im and Avouac., 2021), where an inertia-dominated instability appears as a harmonic oscillation in our elastoplastic wedge (i.e., upper plate). This inertia-dominated instability may enhance the slip/backslip on the interface, similar to the effect of “dynamic shaking” on the plate interface coupling in Southern Cascadia (Materna et al., 2019).

#### 4.2 Effect of the model slab acceleration on the rapid relocking

Our simplified seismotectonic megathrust model suggests different rebounds (i.e., in terms of timing, magnitude, and direction) in the upper plate and slab, triggering the immediate early-postseismic signals. An immediate relocking starts after rupture arrest and leads to a reversed surface displacement. While the rapid relocking is apparently limited on the two MSPs (in the heterogeneous system), it may postseismically reach a significant amount of the coseismic slip increments. The elastic response of the model slab (“delayed rebound”), which comes into play as local acceleration, speeds up the stress build-up and results in this accelerated backslip. The large normal faulting aftershocks in the model slab following a megathrust event seaward of the megathrust event, such as occurring after the Maule earthquake (Ruiz & Contreras-Reyes, 2015) and the Tohoku-Oki earthquake (Asano *et al.*, 2011; Lay *et al.*, 2011) reflect slab extension and thus the same elastic response of the slab.

While the acceleration's impact appears as landward surface displacements above the MSPs, the surface displacements above the matrix follow the slip sense of the MSPs in the heterogeneous configuration (S2). The significant amount of backslip suggests that the delayed rebound may not be the only possible mechanism involved in the landward surface displacement. An extreme coseismic stress-drop overshoots the strained upper plate trenchward coseismically. The upper plate postseismically responds to this overshoot such that its elastic restoring force drags it back

to a quasi-equilibrium state, which may appear as localized upper plate landward surface displacements to a quasi-equilibrium state (Figure 9).

An immediate relocking and a high backslip velocity have been modeled based on land-limited GPS stations for the 2007 Pisco (Remy et al., 2016) and the 2010 Maule (Bedford et al., 2016) megathrust earthquakes, respectively. In the Tohoku-Oki earthquake region, the sparse sites directly above the high-slip zone postseismically moved landward faster than the pre-earthquake velocity (Tomita et al., 2015). This fast postseismic velocity has been explained via a slab acceleration driven by the recovery of force balance (Heki & Mitsui, 2013; Yuzariyadi & Heki, 2021) and the mantle relaxation (Sun et al., 2014; Watanabe et al., 2014). But it is expected that the mantle relaxation affects surface velocities at a relatively large wavelength. Also, the viscoelastic relaxation could not explain the trenchward motion of the stations above the slip zone further landward from the trench (Yuzariyadi & Heki, 2021). Afterslip might be the responsible mechanism for this surface displacement contrast at a relatively short distance (e.g., Sun & Wang, 2015; Tomita et al., 2017). Nevertheless, the coarse sampling rate of near-source observations prevents monitoring how the signals appear and evolve. Our analog model supports the occurrence of significant postseismic velocity changes with the model slab deceleration following Omori-Utsu's decay law (Figure S4) of aftershock activity (Utsu et al., 1995). However, any viscoelastic behavior of the mantle may modify the elastic response of the model slab and lead to a different response time scale. It means that the acceleration may last longer postseismically and decay with another characteristic time-constant in a coupled brittle-viscous system.

The stress evolution model for the extreme weakening observed during the Tohoku-Oki earthquake suggests a 20% slip reversal in the rupture's final stage, consistent with the postseismic stress stage derived from breakout data (Brodsky et al., 2017, 2020). However, our models suggest that the localized slip reversal may reflect the early postseismic stage due to a model slab acceleration and/or a rapid restoration of the upper plate after experiencing elastic overshooting. Moreover, a dynamic slip reversal was reported in the 2011 Mw 9.0 Tohoku-Oki earthquake by Ide et al. (2011). It has been suggested that the reversal of rupture propagation direction (from updip to downdip) and amplified upper plate displacement is caused by coseismic dynamic overshooting, which is consistent with our experimental observation. If the mechanisms of these observations in our experiment and the case of Tohoku-Oki earthquake are compatible, the normal

mechanism aftershocks on the interface close to the maximum slip area (Ide et al., 2011; Yagi & Fukahata, 2011) may be comparable to our proposed early postseismic backslip.

#### 4.3 Effects of the acceleration on the upper plate fault activity

Apart from the consequences on asperities, the accelerated relocking also affects upper-plate shortening and upper-plate fault activity. The antithetic fault in our experiments switches its kinematic mode and acts as a normal fault coseismically due to its location relative to the megathrust earthquake centroid (e.g., deDontney et al., 2012; Li et al., 2014; Xu et al., 2015). This discontinuity inside the upper plate responds to stress perturbation and stress enhancement. When the MSPs are in opposite modes in the heterogeneous system (loading vs. unloading), they cause compressional (postseismically) and extensional (coseismically and/or early postseismically) stress regimes on the two segments of the antithetic upper plate fault, respectively. The high amount of the early postseismic shortening (Figure S5; postseismic/interseismic=20-25%) may increase the stress level in the upper plate, which is consistent with the reported upper-plate seismicity after megathrust earthquakes (e.g., Asano et al., 2011; Hoskins et al., 2021; Toda et al., 2011).

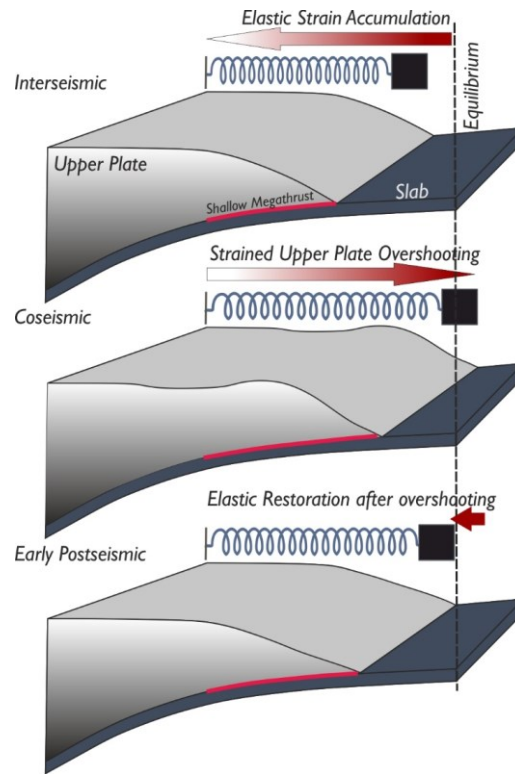


**Figure 9.** Schematic diagram of upper plate elastic behavior during coseismic overshooting and postseismic restoration. The interseismically strained upper plate is overshoot trenchward (seaward) due to an extreme coseismic stress-drop on the interface. Subsequently, an elastic restoring force drags the upper plate back to its equilibrium state.

#### 4.4 Effects of the acceleration on event triggering

The early-postseismic  $\Delta$ CFS enhancement in the model slab may increase the tensional load in the model slab (e.g., Lay *et al.*, 1989; Tilmann *et al.*, 2016) such that the postseismic extensional domain hosts the reported large normal mechanism aftershocks early after the megathrust event (e.g., Asano *et al.*, 2011; Lay *et al.*, 2011; Ruiz and Contreras-Reyes, 2015). The stress enhancement on either receiver MSP (direct effect) or subducting plate (indirect effect) may bring the second MSP close to failure. In the heterogeneous configuration, the stress drop of the former event enhances  $\Delta$ CFS on the second MSP, such that it directly increases the probability of failure. On the other hand, comparing the timing of model slab acceleration and the latter event ( $t_2$  versus  $t_3$ ) shows that the acceleration occurs ahead of the later event. This interestingly suggests that the acceleration caused by the delayed elastic response of the model slab has antedated the later event



on the shallow MSP (Figures 10 & S6). Hence, the acceleration perturbs the MSP's seismic cycle and causes a “clock advance” in the loading cycle of the MSP (Figures S6 and S7).

The rupture of one asperity enhances the stress changes on the adjacent asperity and may bring it closer to failure. For example, Melnick *et al.* (2017) suggest that, besides static stress changes, the increased locking appears in segments adjacent to the failed asperity due to a combination of viscoelastic mantle relaxation and afterslip-controlled vertical axis rotation in the upper plate. The studies on the Wenchuan-Lushan sequential events on the Longmenshan fault show accelerated healing of asperity in response to an earthquake on the adjacent asperity (Pei *et al.*, 2019; Zhao *et al.*, 2020). Accordingly, the enhanced postseismic compression and the accelerating accumulation of the elastic strain triggered the second event on the nearby asperity (Li *et al.*, 2018).

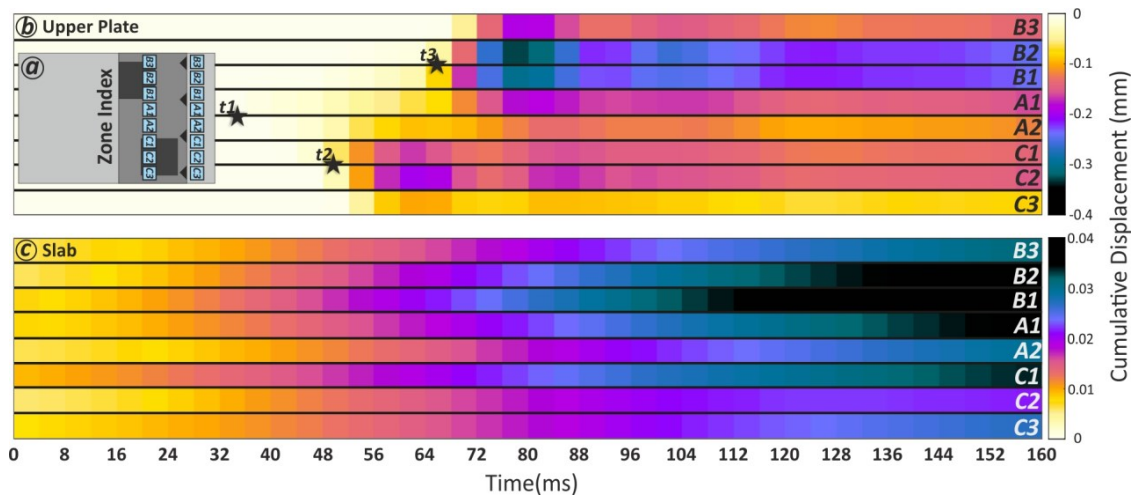


**Figure 10.** Timing of coseismic and postseismic elastic responses of the upper plate and model slab for a representative event. *a*: relative location of the time-series on both plates shown as zone index; *b*: the elastic response of the upper plate. *t1* to *t3* indicates the relative timing of the events; *c*: the elastic response of the slab.

## 5. Conclusion

Our result shows a sequential elastic rebound following the coseismic shear-stress drop in our elastoplastic-frictional models as the rebound of the upper plate is faster and more prominent compared to that of the slab. The delayed rebound of the slab, along with rapid relaxation of the upper plate after an elastic overshooting, may accelerate the relocking of the megathrust. The

laboratory seismogeodetic observations show how the upper plate responds to this overshoot postseismically such that the elastic restoring force may appear as localized upper plate rearward surface displacements. This acceleration triggers/antedates the failure of a nearby asperity and enhances the early backslip in the rupture area. However, depending on the scaling factors, this sequence of dynamic overshooting, amplified motion of the upper plate, and upper plate rearward restoration may alternatively be considered as the coseismic phase. We suggest that the immediate backslip following the main event on the patches could reach up to 30% of coseismic slip and the entire interseismic backslip. The slip models of the upper plate fault demonstrate that the different segments of the upper plate backthrust may move in opposite directions (normal versus reverse), reflecting the sense of shear on the MSPs (slip versus backslip). This deep-rooted backthrust fault generates a discontinuity in the upper plate and perturbs the inner-wedge stress state. Consequently, the discontinuity may strongly enhance the  $\Delta\text{CFS}$  in the upper plate.

## Acknowledgment

The research is supported by the SUBITOP Marie Skłodowska-Curie Action project from the European Union's EU Framework Programme for Research and Innovation Horizon 2020 (Grant Agreement 674899) and partially funded by Deutsche Forschungsgemeinschaft (DFG) through Grant CRC 1114 “Scaling Cascades in Complex Systems,” Project 235221301, Project (B01). The authors thank M. Rudolf and F. Neumann for their helpful discussion and assistance during our laboratory experiments. We thank the editor, Satoshi Ide, the associate editor of the journal, thank Jack Loveless, and an anonymous reviewer for their constructive reviews that helped us to improve the paper.

## Data Availability Statement

All data in this study are online and published open access in Kosari et al. (2022b) (<https://doi.org/10.5880/fidgeo.2022.024>). We thank GFZ Data Services for publishing the data.

## References

- Adam, J., Urai, J. L., Wieneke, B., Oncken, O., Pfeiffer, K., Kukowski, N., Lohrmann, J., Hoth, S., Van Der Zee, W., & Schmatz, J. (2005). Shear localisation and strain distribution during tectonic faulting—New insights from granular-flow experiments and high-resolution optical image correlation techniques. *Journal of Structural Geology*, 27(2), 283–301.

- Allmendinger, R. W., Reilinger, R., & Loveless, J. (2007). Strain and rotation rate from GPS in Tibet, Anatolia, and the Altiplano. *Tectonics*, 26(3). <https://doi.org/10.1029/2006TC002030>
- Asano, Y., Saito, T., Ito, Y., Shiomi, K., Hirose, H., Matsumoto, T., Aoi, S., Hori, S., & Sekiguchi, S. (2011). Spatial distribution and focal mechanisms of aftershocks of the 2011 off the Pacific coast of Tohoku Earthquake. *Earth, Planets and Space*, 63(7), 669–673. <https://doi.org/10.5047/eps.2011.06.016>
- Bedford, J., Moreno, M., Baez, J. C., Lange, D., Tilmann, F., Rosenau, M., Heidbach, O., Oncken, O., Bartsch, M., Rietbrock, A., Tassara, A., Bevis, M., & Vigny, C. (2013). A high-resolution, time-variable afterslip model for the 2010 Maule Mw = 8.8, Chile megathrust earthquake. *Earth and Planetary Science Letters*, 383, 26–36. <https://doi.org/10.1016/j.epsl.2013.09.020>
- Bedford, J., Moreno, M., Li, S., Oncken, O., Baez, J. C., Bevis, M., Heidbach, O., & Lange, D. (2016). Separating rapid relocking, afterslip, and viscoelastic relaxation: An application of the postseismic straightening method to the Maule 2010 cGPS. *Journal of Geophysical Research: Solid Earth*, 121(10), 7618–7638. <https://doi.org/10.1002/2016JB013093>
- Bedford, J. R., Moreno, M., Deng, Z., Oncken, O., Schurr, B., John, T., Báez, J. C., & Bevis, M. (2020). Months-long thousand-kilometre-scale wobbling before great subduction earthquakes. *Nature* 2020 580:7805, 580(7805), 628–635. <https://doi.org/10.1038/s41586-020-2212-1>
- Bilek, S. L., & Lay, T. (2002). Tsunami earthquakes possibly widespread manifestations of frictional conditional stability. *Geophysical Research Letters*, 29(14), 18–1. <https://doi.org/10.1029/2002GL015215>
- Brodsky, E. E., Mori, J. J., Anderson, L., Chester, F. M., Conin, M., Dunham, E. M., Eguchi, N., Fulton, P. M., Hino, R., Hirose, T., Ikari, M. J., Ishikawa, T., Jeppson, T., Kano, Y., Kirkpatrick, J., Kodaira, S., Lin, W., Nakamura, Y., Rabinowitz, H. S., ... Yang, T. (2020). The State of Stress on the Fault Before, During, and After a Major Earthquake. *Annual Review of Earth and Planetary Sciences*, 48(1), 49–74. <https://doi.org/10.1146/annurev-earth-053018-060507>
- Brodsky, E. E., Saffer, D., Fulton, P., Chester, F., Conin, M., Huffman, K., Moore, J. C., & Wu, H.-Y. (2017). The postearthquake stress state on the Tohoku megathrust as constrained by reanalysis of the JFAST breakout data. *Geophysical Research Letters*, 44(16), 8294–8302. <https://doi.org/10.1002/2017GL074027>
- Caniven, Y., & Dominguez, S. (2021). Validation of a Multilayered Analog Model Integrating Crust-Mantle Visco-Elastic Coupling to Investigate Subduction Megathrust Earthquake Cycle. *Journal of Geophysical Research: Solid Earth*, 126(2), e2020JB020342. <https://doi.org/10.1029/2020JB020342>
- Chaves, E. J., Schwartz, S. Y., & Abercrombie, R. E. (2020). Repeating earthquakes record fault weakening and healing in areas of megathrust postseismic slip. *Science Advances*, 6(32), eaaz9317. <https://doi.org/10.1126/sciadv.aaz9317>
- Chlieh, M., Avouac, J. P., Sieh, K., Natawidjaja, D. H., & Galetzka, J. (2008). Heterogeneous coupling of the Sumatran megathrust constrained by geodetic and paleogeodetic measurements. *Journal of Geophysical Research: Solid Earth*, 113, 5305. <https://doi.org/10.1029/2007JB004981>
- Corbi, F., Sandri, L., Bedford, J., Funicello, F., Brizzi, S., Rosenau, M., & Lallemand, S. (2019). Machine Learning Can Predict the Timing and Size of Analog Earthquakes. *Geophysical Research Letters*, 46(3), 1303–1311. <https://doi.org/10.1029/2018GL081251>

- Corbi, Fabio, Bedford, J., Sandri, L., Funiciello, F., Gualandi, A., & Rosenau, M. (2020). Predicting imminence of analog megathrust earthquakes with Machine Learning: Implications for monitoring subduction zones. *Geophysical Research Letters*, 47(7), e2019GL086615. <https://doi.org/10.1029/2019GL086615>
- Corbi, Fabio, Herrendörfer, R., Funiciello, F., & van Dinther, Y. (2017). Controls of seismogenic zone width and subduction velocity on interplate seismicity: Insights from analog and numerical models. *Geophysical Research Letters*, 44(12), 6082–6091. <https://doi.org/10.1002/2016GL072415>
- deDontney, N., Rice, J. R., & Dmowska, R. (2012). Finite element modeling of branched ruptures including off-fault plasticity. *Bulletin of the Seismological Society of America*, 102(2), 541–562. <https://doi.org/10.1785/0120110134>
- Gao, X., & Wang, K. (2017). Rheological separation of the megathrust seismogenic zone and episodic tremor and slip. *Nature* 2017 543:7645, 543(7645), 416–419. <https://doi.org/10.1038/nature21389>
- Heki, K., & Mitsui, Y. (2013). Accelerated pacific plate subduction following interplate thrust earthquakes at the Japan trench. *Earth and Planetary Science Letters*, 363, 44–49. <https://doi.org/10.1016/j.epsl.2012.12.031>
- Herman, M. W., & Govers, R. (2020). Stress evolution during the megathrust earthquake cycle and its role in triggering extensional deformation in subduction zones. *Earth and Planetary Science Letters*, 544, 116379. <https://doi.org/10.1016/J.EPSL.2020.116379>
- Hicks, S. P., & Rietbrock, A. (2015). Seismic slip on an upper-plate normal fault during a large subduction megathrust rupture. *Nature Geoscience*, 8(12), 955–960. <https://doi.org/10.1038/ngeo2585>
- Hoffmann, F., Metzger, S., Moreno, M., Deng, Z., Sippl, C., Ortega-Culaciati, F., & Oncken, O. (2018). Characterizing Afterslip and Ground Displacement Rate Increase Following the 2014 Iquique-Pisagua Mw 8.1 Earthquake, Northern Chile. *Journal of Geophysical Research: Solid Earth*, 123(5), 4171–4192. <https://doi.org/10.1002/2017JB014970>
- Hoskins, M. C., Meltzer, A., Font, Y., Agurto-Detzel, H., Vaca, S., Rolandone, F., Nocquet, J. M., Soto-Cordero, L., Stachnik, J. C., Beck, S., Lynner, C., Ruiz, M., Alvarado, A., Hernandez, S., Charvis, P., Regnier, M., Leon-Rios, S., & Rietbrock, A. (2021). Triggered crustal earthquake swarm across subduction segment boundary after the 2016 Pedernales, Ecuador megathrust earthquake. *Earth and Planetary Science Letters*, 553, 116620. <https://doi.org/10.1016/j.epsl.2020.116620>
- Hsu, Y. J., Simons, M., Avouac, J. P., Galetka, J., Sieh, K., Chlieh, M., Natawidjaja, D., Prawirodirdjo, L., & Bock, Y. (2006). Frictional afterslip following the 2005 Nias-Simeulue earthquake, Sumatra. *Science*, 312(5782), 1921–1926. <https://doi.org/10.1126/science.1126960>
- Ide, S., Baltay, A., & Beroza, G. C. (2011). Shallow dynamic overshoot and energetic deep rupture in the 2011 M w 9.0 Tohoku-Oki earthquake. *Science*, 332(6036), 1426–1429. <https://doi.org/10.1126/science.1207020>
- Im, K., & Avouac, J. P. (2021). Tectonic tremor as friction-induced inertial vibration. *Earth and Planetary Science Letters*, 576, 117238. <https://doi.org/10.1016/J.EPSL.2021.117238>
- Im, K., Marone, C., & Elsworth, D. (2019). The transition from steady frictional sliding to inertia-dominated instability with rate and state friction. *Journal of the Mechanics and Physics of Solids*, 122, 116–125. <https://doi.org/10.1016/J.JMPS.2018.08.026>
- Kato, A., Sakai, S., & Obara, K. (2011). A normal-faulting seismic sequence triggered by the

- 2011 off the Pacific coast of Tohoku Earthquake: Wholesale stress regime changes in the upper plate. *Earth, Planets and Space*, 63(7), 745–748.  
<https://doi.org/10.5047/eps.2011.06.014>
- King Hubbert, M. (1937). Theory of scale models as applied to the study of geologic structures. *Bulletin of the Geological Society of America*, 48(10), 1459–1520.  
<https://doi.org/10.1130/GSAB-48-1459>
- Kosari, E., Rosenau, M., Bedford, J., Rudolf, M., & Oncken, O. (2020). On the Relationship Between Offshore Geodetic Coverage and Slip Model Uncertainty: Analog Megathrust Earthquake Case Studies. *Geophysical Research Letters*, 47(15).  
<https://doi.org/10.1029/2020GL088266>
- Kosari, E., Rosenau, M., & Oncken, O. (2022a). Strain Signals Governed by Frictional-Elastoplastic Interaction of the Upper Plate and Shallow Subduction Megathrust Interface Over Seismic Cycles. *Tectonics*, 41(5), e2021TC007099.  
<https://doi.org/10.1029/2021TC007099>
- Kosari, E; Rosenau, M; Ziegenhagen, T; Oncken, O (2022b): High-speed digital image correlation data from laboratory subduction megathrust models. GFZ Data Services.  
<https://doi.org/10.5880/fidgeo.2022.024>
- Lay, T., Ammon, C. J., Kanamori, H., Kim, M. J., & Xue, L. (2011). Outer trench-slope faulting and the 2011 Mw 9.0 off the Pacific coast of Tohoku Earthquake. *Earth, Planets and Space*, 63(7), 713–718. <https://doi.org/10.5047/eps.2011.05.006>
- Lay, T., Astiz, L., Kanamori, H., & Christensen, D. H. (1989). Temporal variation of large intraplate earthquakes in coupled subduction zones. *Physics of the Earth and Planetary Interiors*, 54(3–4), 258–312. [https://doi.org/10.1016/0031-9201\(89\)90247-1](https://doi.org/10.1016/0031-9201(89)90247-1)
- Li, S., Moreno, M., Bedford, J., Rosenau, M., & Oncken, O. (2015). Revisiting viscoelastic effects on interseismic deformation and locking degree: A case study of the Peru-North Chile subduction zone. *Journal of Geophysical Research: Solid Earth*, 120(6), 4522–4538.  
<https://doi.org/10.1002/2015JB011903>
- Li, S., Moreno, M., Rosenau, M., Melnick, D., & Oncken, O. (2014). Splay fault triggering by great subduction earthquakes inferred from finite element models. *Geophysical Research Letters*, 41(2), 385–391. <https://doi.org/10.1002/2013GL058598>
- Li, Y., Zhang, G., Shan, X., Liu, Y., Wu, Y., Liang, H., Qu, C., & Song, X. (2018). GPS-Derived Fault Coupling of the Longmenshan Fault Associated with the 2008 Mw Wenchuan 7.9 Earthquake and Its Tectonic Implications. *Remote Sensing*, 10(5), 753.  
<https://doi.org/10.3390/rs10050753>
- Lin, J., & Stein, R. S. (2004). Stress triggering in thrust and subduction earthquakes and stress interaction between the southern San Andreas and nearby thrust and strike-slip faults. *Journal of Geophysical Research: Solid Earth*, 109(B2).  
<https://doi.org/10.1029/2003jb002607>
- Loveless, J. P. (2017). Super-interseismic periods: Redefining earthquake recurrence. In *Geophysical Research Letters* (Vol. 44, Issue 3, pp. 1329–1332). Blackwell Publishing Ltd.  
<https://doi.org/10.1002/2017GL072525>
- Loveless, J. P., & Meade, B. J. (2011). Spatial correlation of interseismic coupling and coseismic rupture extent of the 2011 MW = 9.0 Tohoku-oki earthquake. *Geophysical Research Letters*, 38(17), 17306. <https://doi.org/10.1029/2011GL048561>
- Luo, H., & Wang, K. (2021). Postseismic geodetic signature of cold forearc mantle in subduction zones. *Nature Geoscience* 2021 14:2, 14(2), 104–109. <https://doi.org/10.1038/s41561-020->

- 00679-9
- Ma, S., & Beroza, G. C. (2008). Rupture Dynamics on a Bimaterial Interface for Dipping Faults. *Bulletin of the Seismological Society of America*, 98(4), 1642–1658. <https://doi.org/10.1785/0120070201>
- Materna, K., Bartlow, N., Wech, A., Williams, C., & Bürgmann, R. (2019). Dynamically Triggered Changes of Plate Interface Coupling in Southern Cascadia. *Geophysical Research Letters*, 46(22), 12890–12899. <https://doi.org/10.1029/2019GL084395>
- Melnick, D., Moreno, M., Quinteros, J., Baez, J. C., Deng, Z., Li, S., & Oncken, O. (2017). The super-interseismic phase of the megathrust earthquake cycle in Chile. *Geophysical Research Letters*, 44(2), 784–791. <https://doi.org/10.1002/2016GL071845>
- Moreno, M., Rosenau, M., & Oncken, O. (2010). 2010 Maule earthquake slip correlates with pre-seismic locking of Andean subduction zone. *Nature* 2010 467:7312, 467(7312), 198–202. <https://doi.org/10.1038/nature09349>
- Pei, S., Niu, F., Ben-Zion, Y., Sun, Q., Liu, Y., Xue, X., Su, J., & Shao, Z. (2019). Seismic velocity reduction and accelerated recovery due to earthquakes on the Longmenshan fault. *Nature Geoscience*, 12(5), 387–392.
- Pohlenz, A., Rudolf, M., Kemnitz, H., & Rosenau, M. (2020). Ring shear test data of glass beads 40-70  $\mu\text{m}$  used for analogue experiments in the Helmholtz Laboratory for Tectonic Modelling (HelTec) at the GFZ German Research Centre for Geosciences in Potsdam.
- Ramberg, H. (1967). Model Experimentation of the Effect of Gravity on Tectonic Processes. *Geophysical Journal International*, 14(1–4), 307–329. <https://doi.org/10.1111/J.1365-246X.1967.TB06247.X>
- Reid, H. F. (1910). The mechanism of the earthquake, the california earthquake of April 18, 1906, Report of the state earthquake investigation commission. In *Washington DC: Carnegie Institution* (Vol. 2).
- Remy, D., Perfettini, H., Cotte, N., Avouac, J. P., Chlieh, M., Bondoux, F., Sladen, A., Tavera, H., & Socquet, A. (2016). Postseismic relocking of the subduction megathrust following the 2007 Pisco, Peru, earthquake. *Journal of Geophysical Research: Solid Earth*, 121(5), 3978–3995. <https://doi.org/10.1002/2015JB012417>
- Rosenau, M., Corbi, F., & Dominguez, S. (2017). Analogue earthquakes and seismic cycles: experimental modelling across timescales. *Solid Earth, European Geosciences Union*. 8(3), 597–635. <https://doi.org/10.5194/se-8-597-2017>
- Rosenau, M., Horenko, I., Corbi, F., Rudolf, M., Kornhuber, R., & Oncken, O. (2019). Synchronization of Great Subduction Megathrust Earthquakes: Insights From Scale Model Analysis. *Journal of Geophysical Research: Solid Earth*, 124(4), 3646–3661. <https://doi.org/10.1029/2018JB016597>
- Rosenau, M., Lohrmann, J., & Oncken, O. (2009). Shocks in a box: An analogue model of subduction earthquake cycles with application to seismotectonic forearc evolution. *Journal of Geophysical Research: Solid Earth*, 114(B1), 1409. <https://doi.org/10.1029/2008JB005665>
- Rosenau, M., Nerlich, R., Brune, S., & Oncken, O. (2010). Experimental insights into the scaling and variability of local tsunamis triggered by giant subduction megathrust earthquakes. *Journal of Geophysical Research: Solid Earth*, 115(9). <https://doi.org/10.1029/2009JB007100>
- Rosenau, M., & Oncken, O. (2009). Fore-arc deformation controls frequency-size distribution of megathrust earthquakes in subduction zones. *Journal of Geophysical Research*, 114(B10),

- B10311. <https://doi.org/10.1029/2009JB006359>
- Ruff, L. J., & Tichelaar, B. W. (1996). What Controls the Seismogenic Plate Interface in Subduction Zones? *Geophysical Monograph Series*, 96, 105–111. <https://doi.org/10.1029/GM096P0105>
- Ruiz, J. A., & Contreras-Reyes, E. (2015). Outer rise seismicity boosted by the Maule 2010 Mw 8.8 megathrust earthquake. *Tectonophysics*, 653, 127–139. <https://doi.org/10.1016/j.tecto.2015.04.007>
- Savage, J. C. (1983). A dislocation model of strain accumulation and release at a subduction zone. *Journal of Geophysical Research*, 88(B6), 4984–4996. <https://doi.org/10.1029/JB088iB06p04984>
- Schmalzle, G. M., McCaffrey, R., & Creager, K. C. (2014). Central Cascadia subduction zone creep. *Geochemistry, Geophysics, Geosystems*, 15(4), 1515–1532. <https://doi.org/10.1002/2013GC005172>
- Schulze, D. (1994). Development and application of a novel ring shear tester. *Aufbereitungs Technik*, 35(10), 524–535.
- Simons, M., Minson, S. E., Sladen, A., Ortega, F., Jiang, J., Owen, S. E., Meng, L., Ampuero, J.-P., Wei, S., Chu, R., Helmberger, D. V., Kanamori, H., Hetland, E., Moore, A. W., & Webb, F. H. (2011). The 2011 Magnitude 9.0 Tohoku-Oki Earthquake: Mosaicking the Megathrust from Seconds to Centuries. *Science*, 332(6036), 1421–1425. <https://doi.org/10.1126/SCIENCE.1206731>
- Sun, T., & Wang, K. (2015). Viscoelastic relaxation following subduction earthquakes and its effects on afterslip determination. *Journal of Geophysical Research: Solid Earth*, 120(2), 1329–1344. <https://doi.org/10.1002/2014JB011707>
- Sun, T., Wang, K., Iinuma, T., Hino, R., He, J., Fujimoto, H., Kido, M., Osada, Y., Miura, S., Ohta, Y., & Hu, Y. (2014). Prevalence of viscoelastic relaxation after the 2011 Tohoku-oki earthquake. *Nature*, 514(7520), 84–87. <https://doi.org/10.1038/nature13778>
- Tilmann, F., Zhang, Y., Moreno, M., Saul, J., Eckelmann, F., Palo, M., Deng, Z., Babeyko, A., Chen, K., Baez, J. C., Schurr, B., Wang, R., & Dahm, T. (2016). The 2015 Illapel earthquake, central Chile: A type case for a characteristic earthquake? *Geophysical Research Letters*, 43(2), 574–583. <https://doi.org/10.1002/2015GL066963>
- Toda, S., Stein, R. S., & Lin, J. (2011). Widespread seismicity excitation throughout central Japan following the 2011 M=9.0 Tohoku earthquake and its interpretation by Coulomb stress transfer. *Geophysical Research Letters*, 38(7). <https://doi.org/10.1029/2011GL047834> @10.1002/(ISSN)1944-8007.MEGAQUAKE1
- Tomita, F., Kido, M., Ohta, Y., Iinuma, T., & Hino, R. (2017). Along-Trench variation in seafloor displacements after the 2011 Tohoku earthquake. *Science Advances*, 3(7), e1700113. <https://doi.org/10.1126/sciadv.1700113>
- Tomita, F., Kido, M., Osada, Y., Hino, R., Ohta, Y., & Iinuma, T. (2015). First measurement of the displacement rate of the Pacific Plate near the Japan Trench after the 2011 Tohoku-Oki earthquake using GPS/acoustic technique. *Geophysical Research Letters*, 42(20), 8391–8397. <https://doi.org/10.1002/2015GL065746>
- Uchida, N., & Bürgmann, R. (2019). Repeating earthquakes. *Annual Review of Earth and Planetary Sciences*, 47(1), 305–332. <https://doi.org/10.1146/annurev-earth-053018-060119>
- Utsu, T., Ogata, Y., S, R., & Matsu'ura. (1995). The Centenary of the Omori Formula for a Decay Law of Aftershock Activity. *Journal of Physics of the Earth*, 43(1), 1–33. <https://doi.org/10.4294/jpe1952.43.1>

- Wang, K., Hu, Y., & He, J. (2012). Deformation cycles of subduction earthquakes in a viscoelastic Earth. *Nature*, 484(7394), 327–332. <https://doi.org/10.1038/nature11032>
- Watanabe, S., Sato, M., Fujita, M., Ishikawa, T., Yokota, Y., Ujihara, N., & Asada, A. (2014). Evidence of viscoelastic deformation following the 2011 Tohoku-Oki earthquake revealed from seafloor geodetic observation. *Geophysical Research Letters*, 41(16), 5789–5796. <https://doi.org/10.1002/2014GL061134>
- Weiss, J. R., Qiu, Q., Barbot, S., Wright, T. J., Foster, J. H., Saunders, A., Brooks, B. A., Bevis, M., Kendrick, E., Ericksen, T. L., Avery, J., Smalley, R. S., Cimbaro, S. R., Lenzano, L. E., Barón, J., Báez, J. C., & Echalar, A. (2019). Illuminating subduction zone rheological properties in the wake of a giant earthquake. *Science Advances*, 5(12), 6720–6738. <https://doi.org/10.1126/sciadv.aax6720>
- Xu, S., Fukuyama, E., Ben-Zion, Y., & Ampuero, J. P. (2015). Dynamic rupture activation of backthrust fault branching. *Tectonophysics*, 644, 161–183. <https://doi.org/10.1016/j.tecto.2015.01.011>
- Yagi, Y., & Fukahata, Y. (2011). Rupture process of the 2011 Tohoku-oki earthquake and absolute elastic strain release. *Geophysical Research Letters*, 38(19). <https://doi.org/10.1029/2011GL048701>
- Yuzariyadi, M., & Heki, K. (2021). Enhancement of interplate coupling in adjacent segments after recent megathrust earthquakes. *Tectonophysics*, 801, 228719. <https://doi.org/10.1016/j.tecto.2021.228719>
- Zhao, J., Ren, J., Liu, J., Jiang, Z., Liu, X., Liang, H., Niu, A., Yue, C., & Yuan, Z. (2020). Coupling fraction and relocking process of the Longmenshan Fault Zone following the 2008 Mw7.9 Wenchuan earthquake. *Journal of Geodynamics*, 101730.



## Captions:

**Figure 1.** Scheme of the seismotectonic scale model's geometry and configuration: *a* and *b* demonstrate our conceptual systems of coupled spring sliders as depicted by Ruff and Tichelaar, (1996). *b* and *c* represent homogenous and heterogeneous configurations, respectively. The yellow (matrix) and magenta (main slip patch) rectangles demonstrate the seismogenic patches which generate repeating earthquake and megathrust events, respectively. P.D.D. represents the projection of the down-dip limit of the seismogenic patch on the model surface. The small orange rectangles show the different configurations of accelerometers. The frictional behavior of both velocity weakening materials used in the matrix and main slip patch is shown in Figure 2.

**Figure 2.** Shear stress time-series measured in a ring-shear tester during velocity stepping tests under constant normal load (2000 Pa). Stick-slip behavior simulates "seismic cycles" with coseismic and interseismic stress drop (analog earthquakes) and increase.. *a* and *b* (main slip patch in Figure 1) and magenta (matrix in Figure 1) demonstrate the seismogenic (i.e., stick-slip) patches which generate megathrust events and repeating earthquakes, respectively. *c* and *d* show seven seismic cycles from both materials. Note that the recurrence of the repeating earthquake is approximately 20 times shorter than the megathrust event. If scaling is applied to these test data, one second corresponds to 250 years, stress drops would be 10-100 MPa, and friction coefficients consistent with Byerlee friction for the interseismic (~0.6-0.7) and ~0.2 after relocking. Note that we cannot measure friction during catastrophic failure properly in this kind of test.

**Figure 3.** Differentiating Quasi-harmonic oscillation and event-related signals. *a* and *b* represent the scalogram of the signal before and after filtering the quasi-harmonic oscillations out. *c* and *d* are the normal-trench acceleration derived from three sensors located on the wedge (*c* and *d*) and the basal rubber conveyor belt (*e*).

**Figure 4.** Model setup and exemplary evolution of coseismic and early-postseismic surface deformation in two scenarios. a and b: Plan view of the seismotectonic scale models' configurations; Light, medium, and dark gray colors represent the "aseismically" creeping interface, a velocity weakening matrix characterized by microslips ("microseismicity"), and the main slip patch(es) (MSP) where large analog megathrust earthquake slip occurs ("seismogenic zone" or "asperity"), respectively. The red dashed lines (marked by circles) show the profiles along which the cumulative surface displacement is shown in c and d. The gray star represents the location of the initiation of the rupture. The downward vectors indicate the reduction of the cumulative trenchward surface displacement representing surface displacement reversal during the early-postseismic stage interpreted as backslip. The corresponding surface deformation maps derived from the synchronized camera are visualized in figures S1 and S2. The stars on the dashed lines show the selected surface displacement snapshots for slip modeling in Figure 5.

**Figure 5.** Upper panel: Slip models of the selected increments (marked in Figure 1d) in the heterogeneous system for demonstrating slip/backslip distribution in the MSPs and the antithetic upper plate fault. The vectors indicate the relative sense of slip but are not to scale. The dashed rectangles indicate the approximate location of the MSPs before shearing into trapezoids. The lower panel represents three trench-normal profiles of Coulomb failure stress changes ( $\Delta CFS$ ) from the slip model snapshot #12 in the heterogeneous configuration. Inset shows the location of profiles on the model surface.

**Figure 6:** Exemplary clockwise and anticlockwise upper plate rotation during coseismic and early postseismic stages derived from selected surface displacements increments. Their associated surface displacements (E07 and E11) are visualized in Figure S2. Note that the sense of rotation during coseismic and postseismic stages causes divergence and convergence motion above the MSPs in the upper plate.

**Figure 7.** Upper plate time-series overlayed on the model slab time-series (background colormap) from the heterogeneous configuration (see Figure S4 for the homogenous configuration). Note the location of the profiles relative to the upper plate and slab. The vertical lines (E1-E22) indicate abrupt surface displacement changes above the matrix. The warm color shows the landward displacement of the slab. Larger events instigate greater model slab responses (Figure 8).

**Figure 8.** Correlation between the upper plate and model slab trenchward (landward) displacements during coseismic and early-postseismic stages.

**Figure 9.** Schematic diagram of upper plate elastic behavior during coseismic overshooting and postseismic restoration. The interseismically strained upper plate is overshoot trenchward (seaward) due to an extreme coseismic stress-drop on the interface. Subsequently, an elastic restoring force drags the upper plate back to its equilibrium state.

**Figure 10.** Timing of coseismic and postseismic elastic responses of the upper plate and model slab for a representative event. a: relative location of the time-series on both plates shown as zone index; b: the elastic response of the upper plate.  $t_1$  to  $t_3$  indicates the relative timing of the events; c: the elastic response of the slab.

# **Figures:**

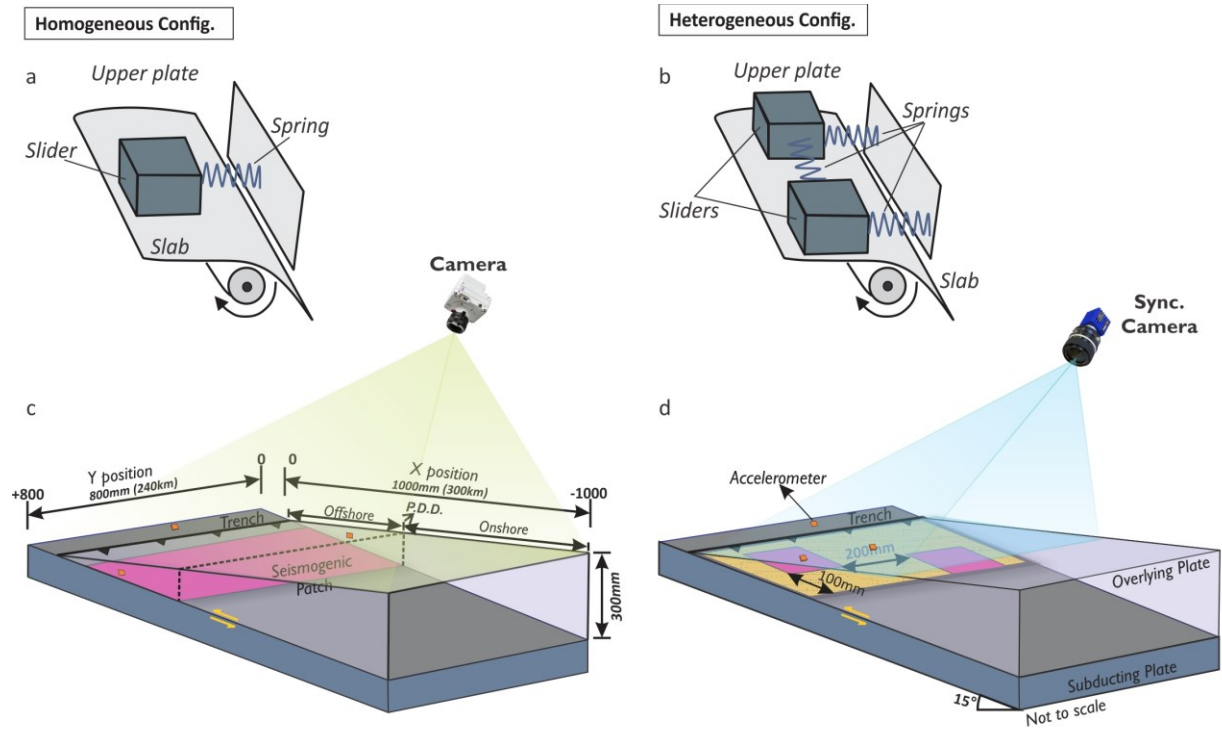


**Figure 1.**

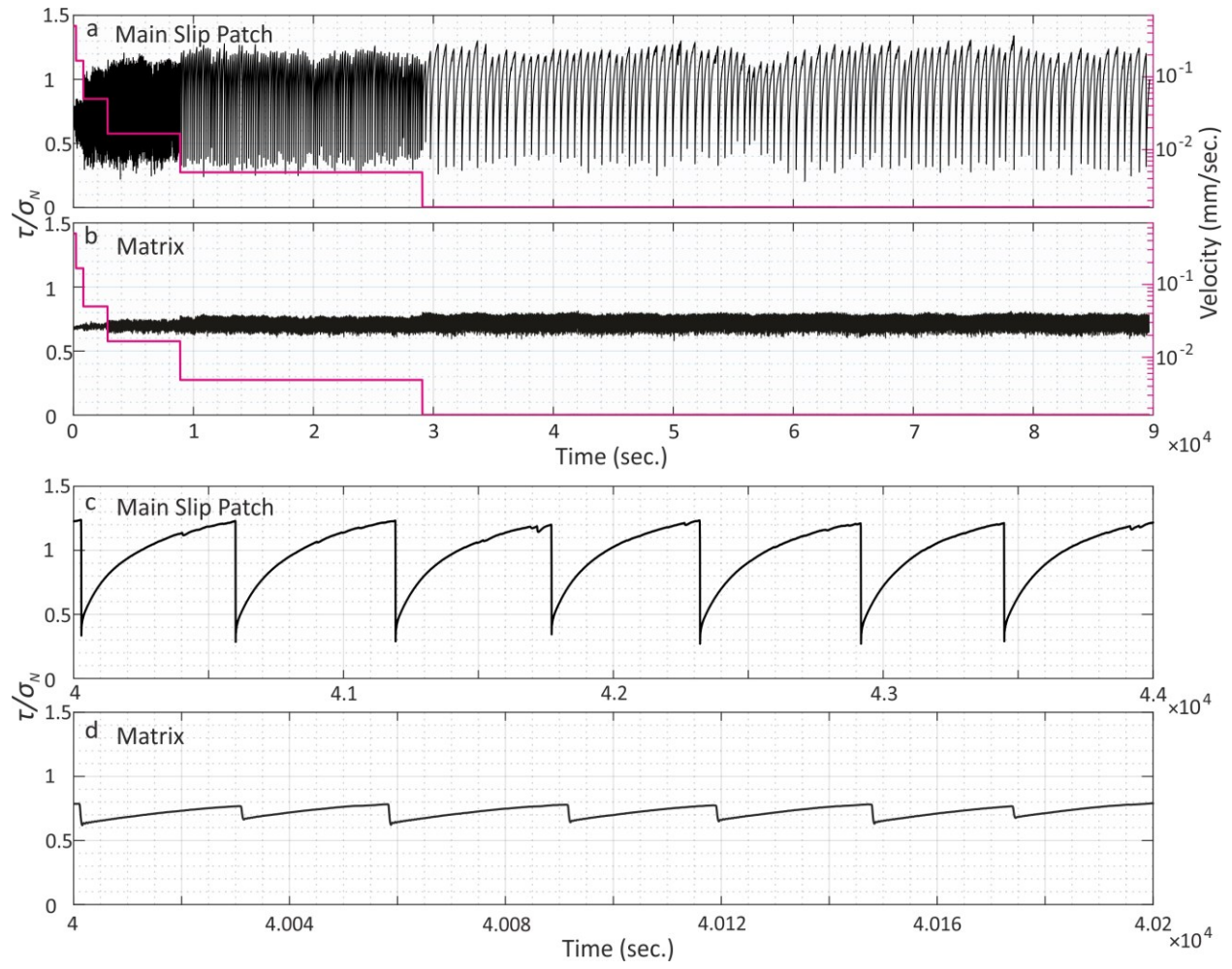


**Figure 2.**

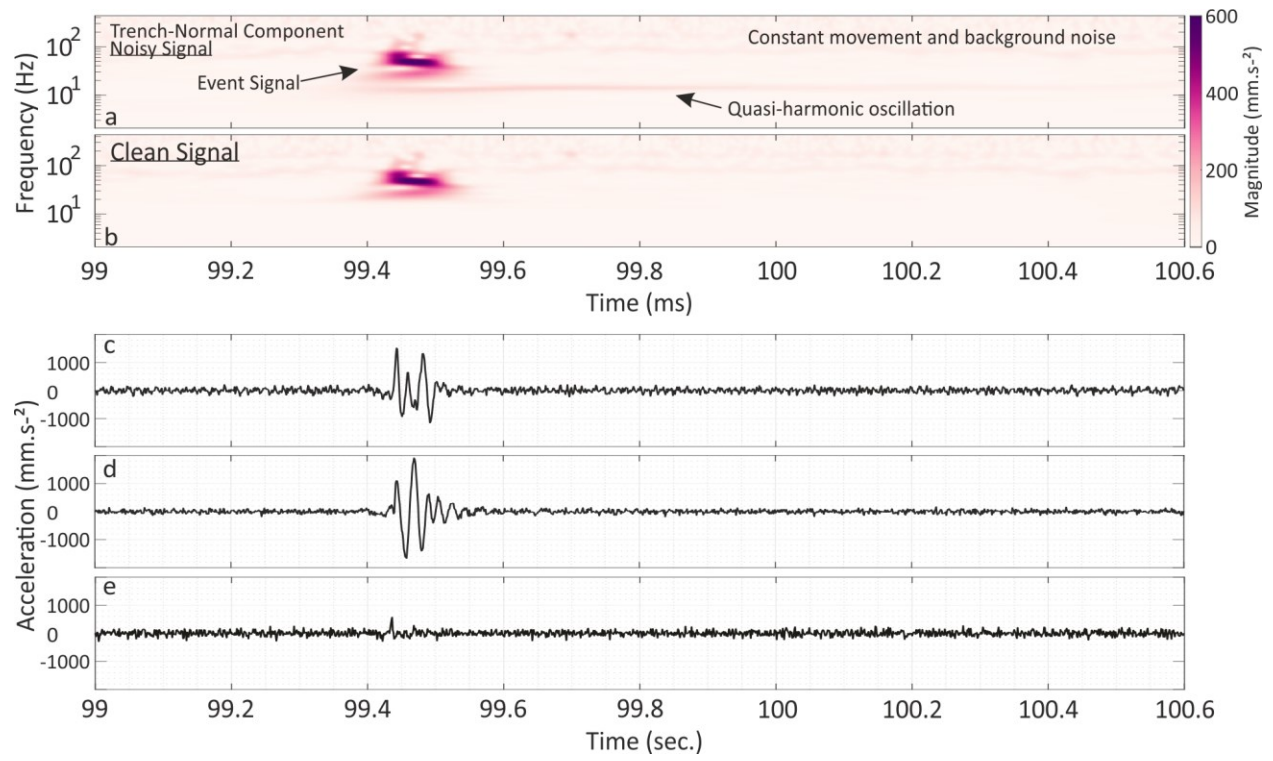


**Figure 3.**

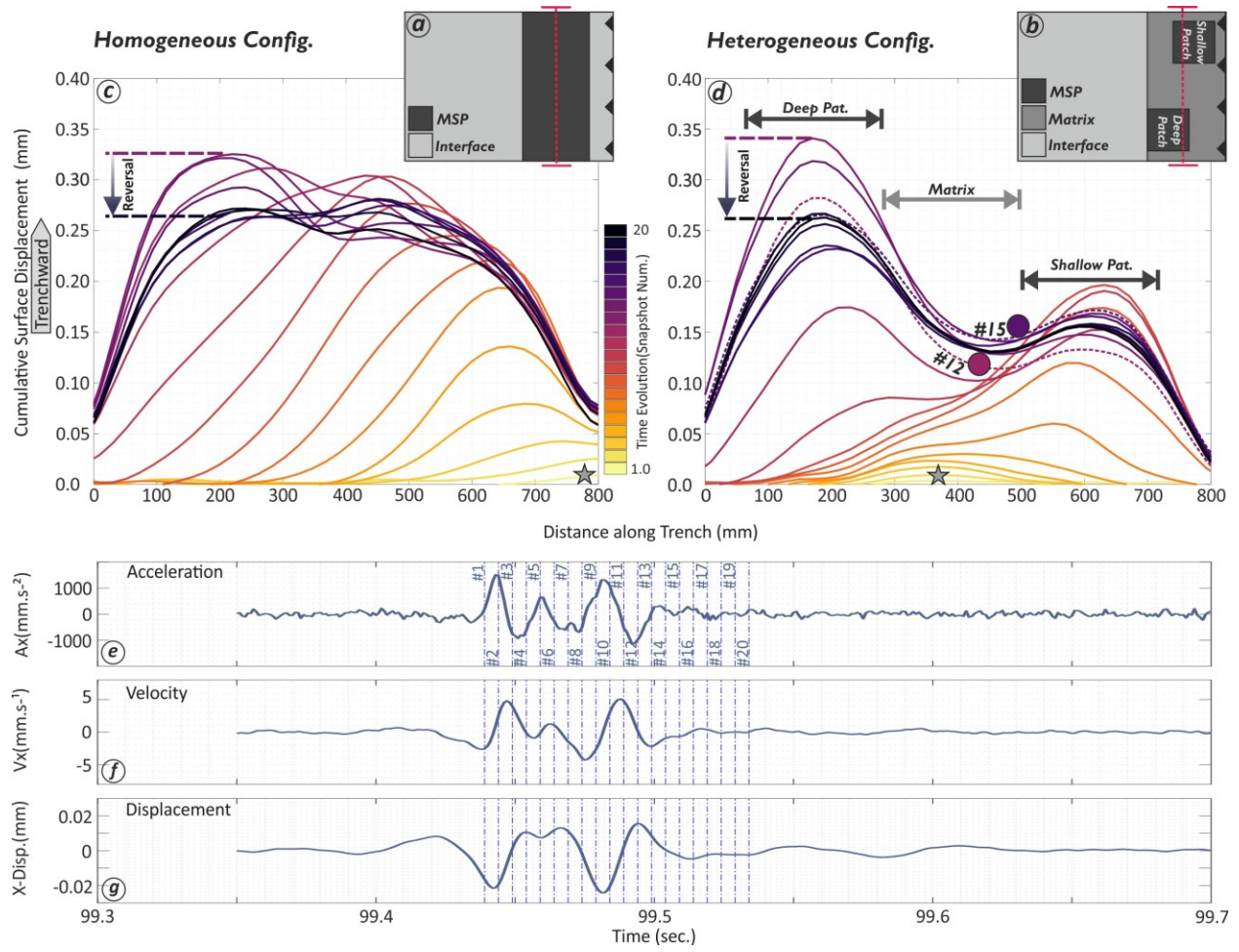


**Figure 4.**



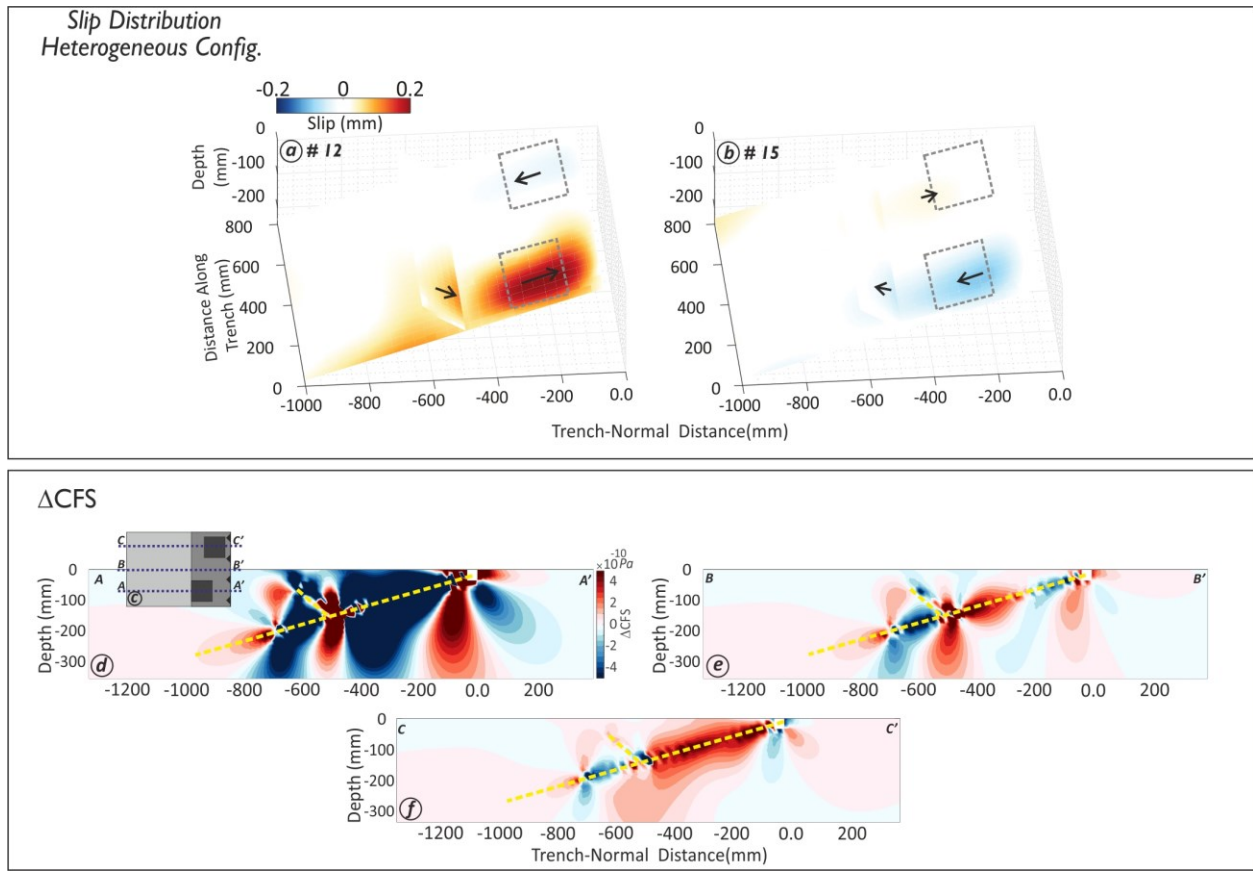


**Figure 5.**



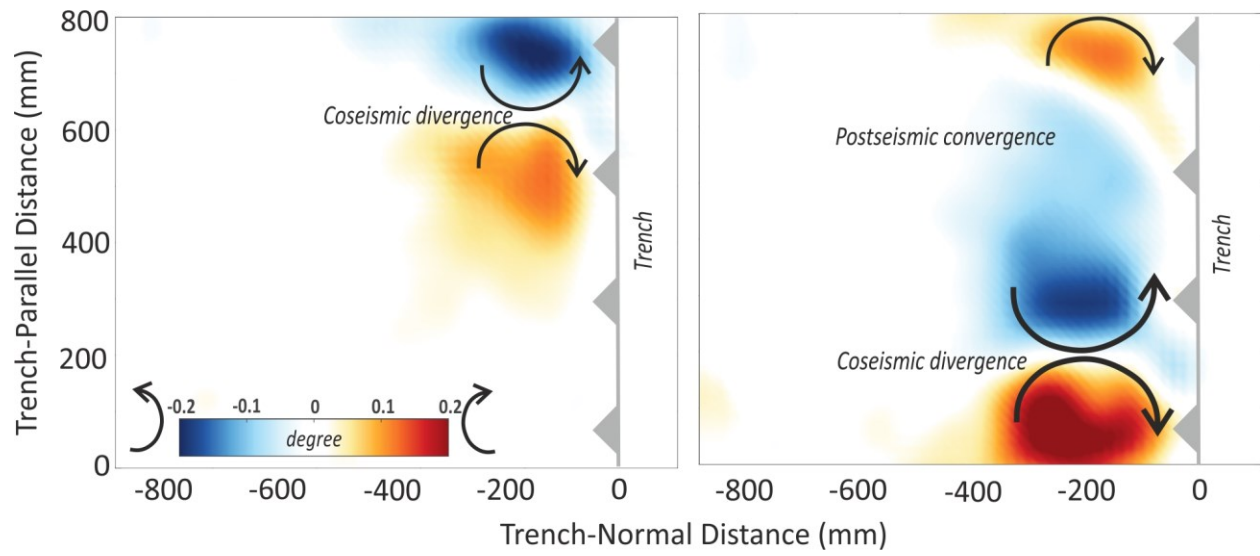


**Figure 6.**

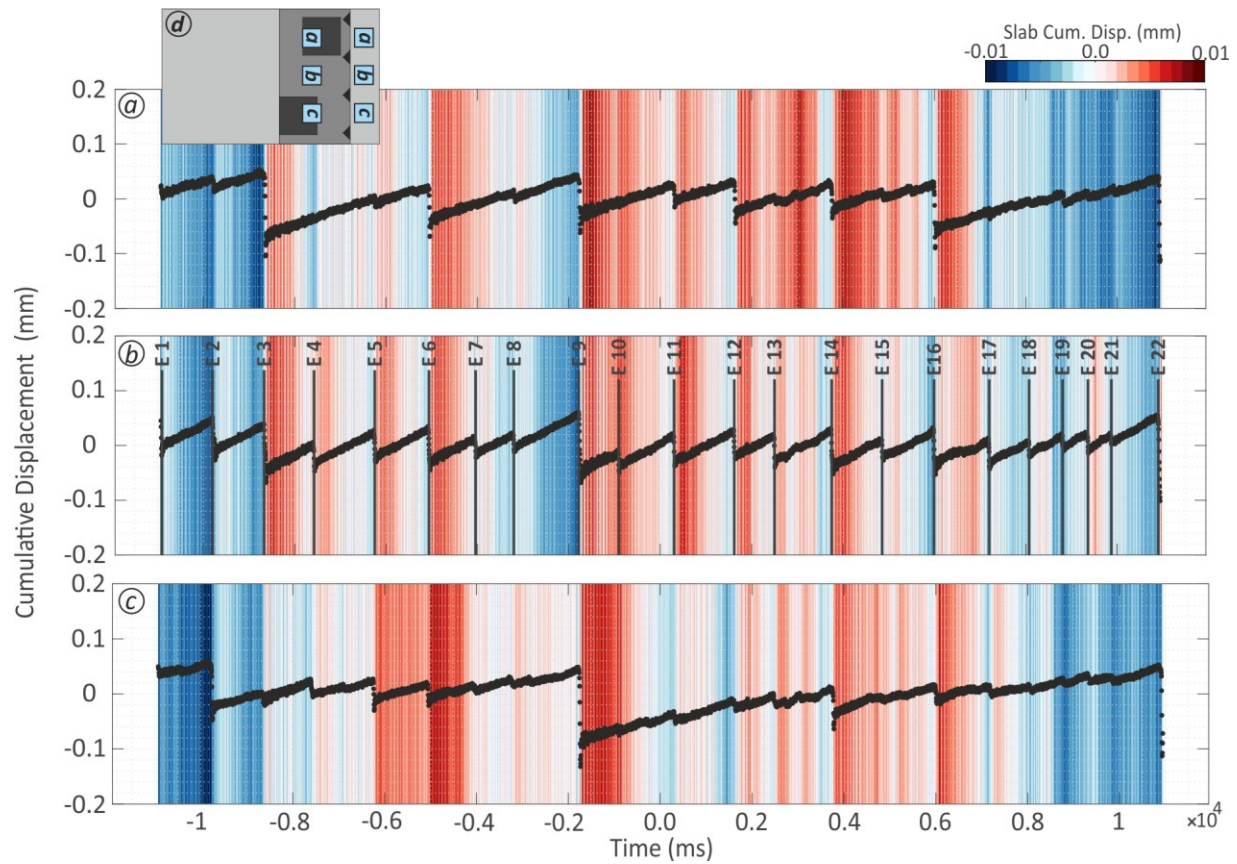


**Figure 7.**

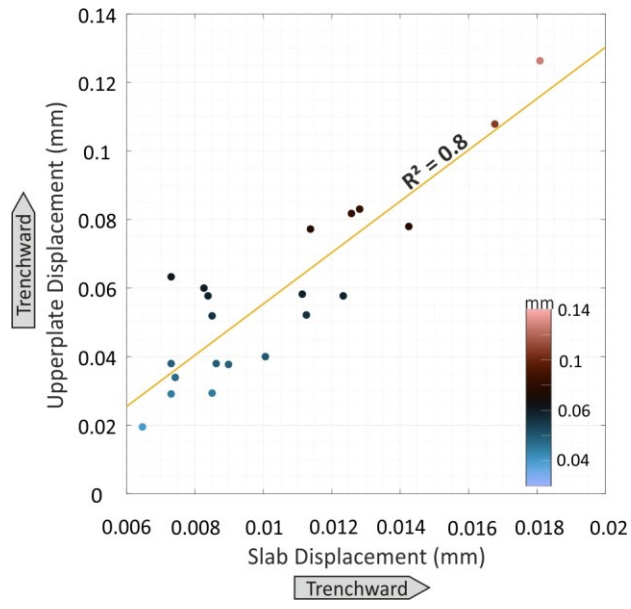


**Figure 8.**

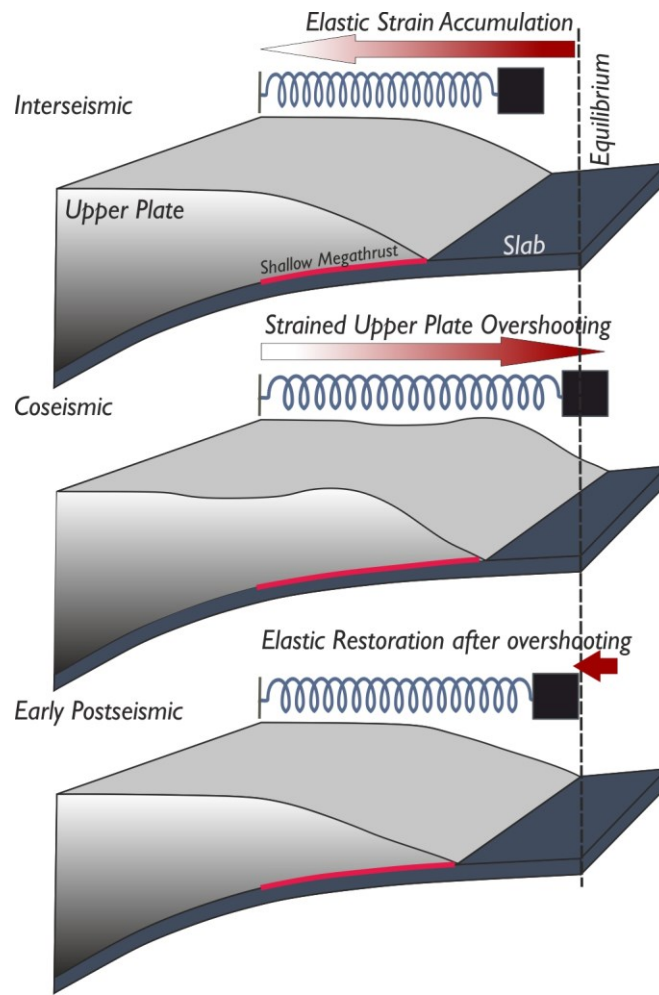


**Figure 9.**

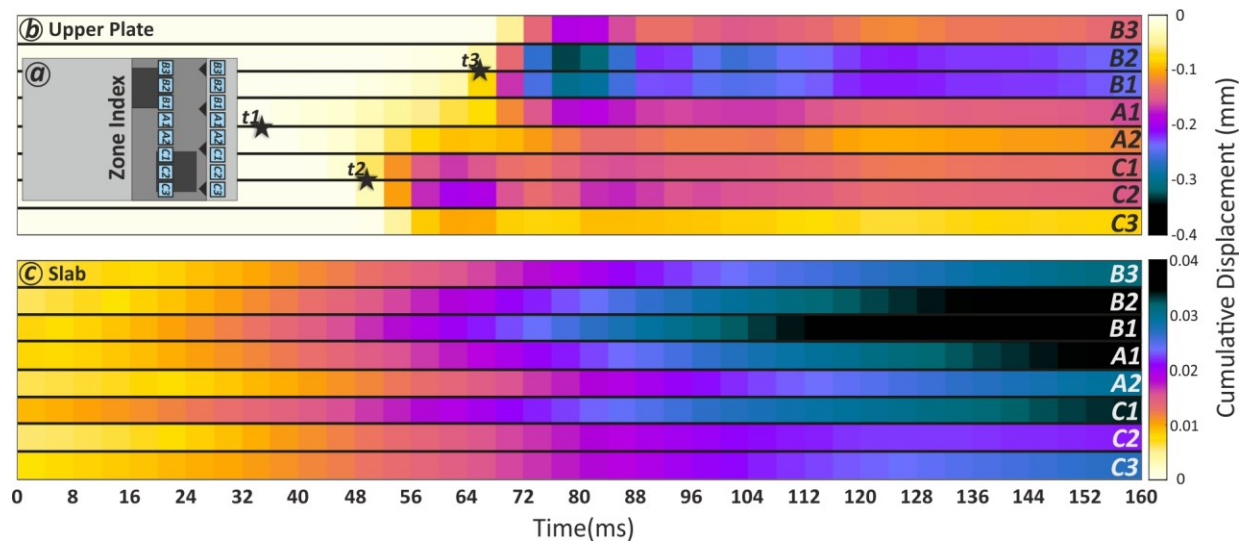


**Figure 10.**